Exploring dynamics of eukaryotic transcription

Rybakova, E.N.

2012

document version
Publisher's PDF, also known as Version of record

Chapter 4

Tracing the molecular basis of altered gene transcription in noisy data by using an experiment-based mathematical model

Changes in transcription-factor levels, epigenetic status, splicing kinetics, and mRNA degradation can each contribute to changes in mRNA dynamics We present a novel method to identify which of these processes is actually changed in cells in response to external signals or as a result of a diseased state. The method employs a mathematical model for which the kinetic rates of gene regulation, splicing, elongation and mRNA degradation, were estimated from noisy experimental data of mRNA dynamics. The dynamics of several intermediates of mRNA synthesis were thereto measured upon activation of the human adipose differentiation-related protein (*ADRP*) gene. We validated the method by monitoring the mRNA dynamics upon gene activation in the presence of a splicing inhibitor. We show that the mathematical model correctly identifies splicing as the inhibitor target, even though the data are very noisy.

4.1 Introduction

mRNA processing is a highly regulated and dynamic process, which is often disturbed in disease (Cooper et al., 2009; Licatalosi and Darnell, 2010; Poulos et al., 2011). Deep-sequencing technology enables high-resolution quantitation of RNA species, such as splicing variants, snRNA, and intermediates in mRNA synthesis. RNA datasets obtained under various conditions may be compared. It has not yet been possible however to infer from differences between such RNA data sets which particular molecular perturbation was at the basis of the alterations in RNA dynamics. If met, the challenge to systems biology of developing methods that infer molecular causes from such datasets, will enable the identification of deregulation processes in cases of disease.

An important tool to this end is the ability to measure mRNA dynamics in cultured cells which has led to many new observations. However, the interpretation of such observations and the elucidation of mechanisms underpinning them, is greatly hampered by the noise in the data (often observed in eukaryotic cell culture experiments) which is obtained in a dynamic, potentially oscillatory context (see Chapter 3). In physics, mathematical models are often sued in such noisy context. They are advantageous not only in that by simulation they can look through the confusion caused by the noise, but, more importantly, in that they enable an objective, more abstract, analysis of the data. This is important when data are potentially oscillatory yet full of noise. Intuitive interpretation then often suggests that there is more of an oscillation than there actually is.

In this chapter we shall obtain noisy experimental data concerning mRNA dynamics and then show how indeed, by using mathematical modelling we can treat the data objectively by comparing the prediction of a number of well-defined models, with the noisy experimental data and then obtaining best fits. The best fits then lead to rejection of some models, persistence of more than one of the other models, and estimates of parameters that are also otherwise important for the understanding of cell biology.

Indeed, mathematical methods for model development on the basis of experimental data, i.e. parameter estimation, model discrimination, and experimental design, offer a rigorous methodology to integrate experimental data on molecular concentrations with molecular network architecture (Aldridge et al., 2006; Ashyraliyev et al., 2009; Cedersund and Roll, 2009;

Kreutz and Timmer, 2009). These methods facilitate the development of rational perturbation strategies and the identification of perturbation targets. They likewise improve our understanding of signalling, metabolic and gene networks, e.g. (Becker et al., 2010; Borisov et al., 2009; Nelson et al., 2004; Schmierer et al., 2008). In this work, we will use these techniques to develop a methodology for modelling that enables inferring the kinetics of the molecular processes underlying mRNA dynamics. We identify the perturbed molecular processes from a comparison of an mRNA time-series of an unperturbed with that of a perturbed cell culture.

We chose to work with the human adipose differentiation-related protein (*ADRP*) gene, which gives a pronounced activation response upon addition of a ligand of its main transcriptional regulator, the peroxisome proliferator-activated receptor delta (PPARδ) (Chang et al., 2006; Fan et al., 2009b; Targett-Adams et al., 2005; Tobin et al., 2006). ADRP (also known as PLIN2 or ADFP) belongs to the family of proteins that associate with the surface of lipid droplets (Targett-Adams et al., 2005). Initially thought to be confined to adipose tissue and to increase during its differentiation process, *ADRP* mRNA was later found in all metabolic tissues (Bildirici et al., 2003). Because nuclear receptors are directly activated by the binding of their cognate ligand to become transcription factors, confounding effects of signaling pathways on mRNA dynamics should be limited. Consequentially *ADRP* should be an attractive system to use for studying the temporal transcription-activation response. We therefore chose to study the dynamics of PPARδ (peroxisome proliferator-activated receptor) controlled expression of the ADRP gene in HepG2 cells.

In parallel we developed a mathematical model that incorporates fundamental processes of mRNA synthesis and processing, such as the promoter *on* and *off* cycle, elongation, splicing, maturation and degradation. Model parameters were estimated by fitting model predictions to our experimental time-courses of RNA species concentrations. We measured an additional time course in the presence of a splicing inhibitor. Re-fitting the model by changing one parameter at a time, we identified a parameter that most likely had been perturbed by the inhibitor. The identified parameter indeed described the splicing process. This study thereby demonstrates how mathematical modelling of transcription can help to identify which molecular processes are perturbed in disease or upon treatment with drugs.

4.2 Results

4.2.1 Model of transcription regulation and mRNA processing and the two operational variables that we can detect

To assess a case of mRNA dynamics we chose the human *ADRP* gene as it can be controlled by the addition of a synthetic ligand of its main transcription factor, the nuclear receptor PPARδ. In preliminary experiments the expression of the *ADRP* in HepG2 cell line depended on PPARδ and responded more than 2-fold to the synthetic PPARδ-ligand GW501516 (Fig. 4.S.2).

The intron-exon organization of the human *ADRP* gene is shown in Figure 4.1.A. In this figure, we also indicate the location of the PCR primers we used to measure various mRNA species over time upon gene activation and transcription inhibition.

The model is schematically shown in Figure 4.1B: it incorporates various features of transcription and RNA processing: regulation of transcription (by transcription factors), the transcription (de-)activation cycle, splicing, elongation, and mRNA degradation. To allow for parameter estimation from experimental data, the model should not contain too many parameters to prevent over fitting and also not too few to make sure it can capture the main features of mRNA dynamics. In the Supplemental Material we outline how we decided on the final mathematical model using a model selection and parameter fitting procedure. The mathematical model is based on ordinary differential equations based on mass-action kinetics. The set of ordinary differential equations describing model from Fig.4.2B are presented in Table 4.1.

We identify two observables by what should be detected by the two main primer pairs we will use. The PCR primer pair marked in blue in Fig. 4.1.A monitors the presence of the first intron, as the right primer lies on the exon-intron boundary. After the splicing step in which this intron is excised, this primer pair will no longer give a PCR product. Therefore this primer pair operationally defines the 'pre-mRNA' of Fig. 4.2, corresponding to the sum of all states of mRNA that still have to be spliced on the first intron. The PCR primer pair indicated in red targets the border of exon 1 and 2 and therefore gives a product only when exon 1 has been excised by splicing. In combination with only measuring polyadenylated fraction of mRNA this primer pair operationally defines what we shall call 'mature' mRNA. We also tested two

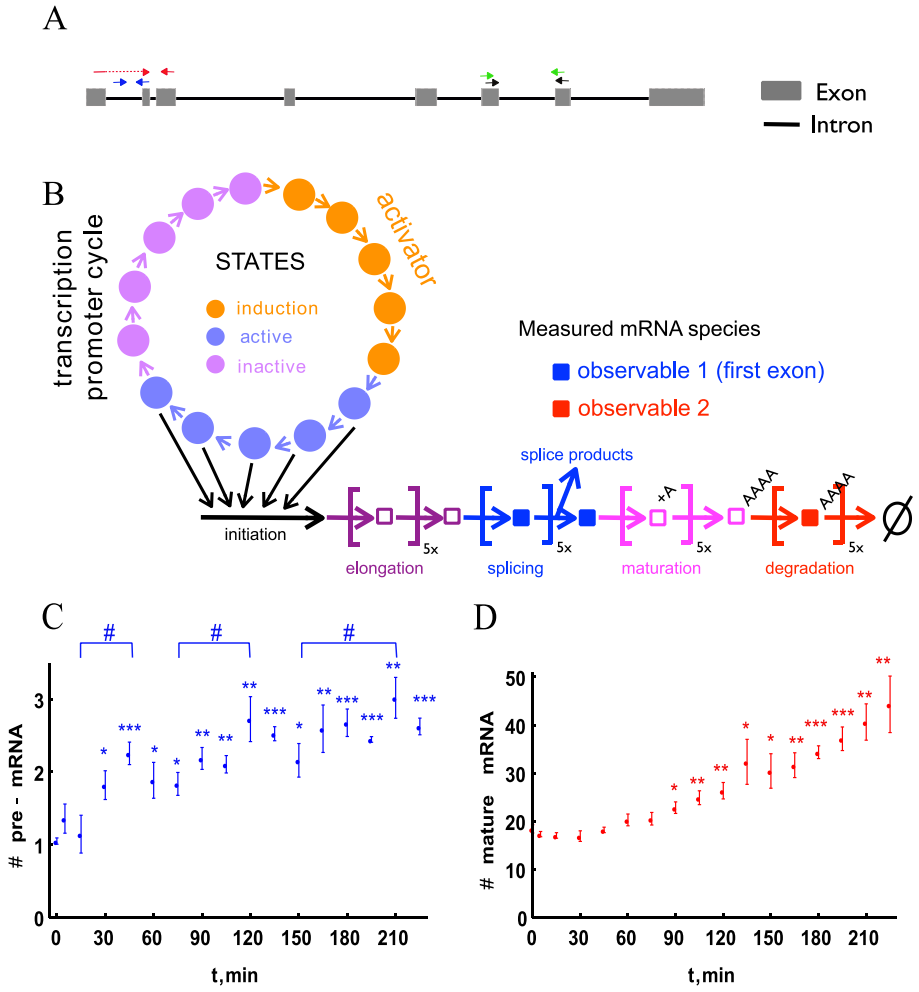

Figure 4.1. Overview of the exon-intron organization of the ADRP gene and the mathematical model of its transcription dynamics. A. Overview of the intron-exon organization of the *ADRP* gene. The length of the gene is indicated in unit base pairs. Exon and introns are denoted as boxes and lines, respectively. The coloured arrows indicate PCR primer pairs. The PCR primer in red overlaps with the right hand side of exon 1 and the left hand side of exon 2. The right PCR primer in blue is situated at the border of intron 1 and exon 2. The green and black primer pairs were tested as well but did not give any additional information on mRNA dynamics (see Supplemental Material). B. Network diagram of the mathematical model of *ADRP* transcription dynamics. The model consists of a 15-state transcription promoter cycle. The five states marked in orange have transition rates that depend on the presence of a transcription activator. The subsequent five 'active' states (marked blue) contribute

equally to transcription initiation. elongation, splicing, maturation, and degradation are all described by five first order steps in a sequence, which represents the stepwise nature of these processes and captures the delays in the experimental data: it takes time before the mRNA species are observed upon gene activation. The third, 'inactive' phase (violet) of promoter state changes independent of the transcription factor activity. In our experiments we will measure two of all the substances in this diagram, i.e. the concentrations of pre-mRNA, i.e. the species before splicing (observable 1), and of mature mRNAs, i.e. the polyadenylated species after splicing (observable 2). Measurement of ADRP transcription dynamics in human HepG2 cells stimulated with 100 nM GW501516: pre-mRNA (A) or mature mRNA (B). Data points represent the means of at least six biological replicate samples corrected for the outliers with MAD method (AMC, 2001), error bars represent the standard error of the mean. Two-tailed, paired Student's t-tests were performed to determine the significance of the ligand-dependent regulation of the *ADRP* RNA in reference to vehicle (*) and in comparison of peaks to the minima (#): *(#)$p<0.05$, **(##)$p<0.01$, ***(###)$p<0.001$.

other primer pairs, marked green and black in Figure 4.1A, but these did not give more information about the mRNA dynamics than the other two PCR primer pairs and were therefore left out of consideration here (see Supplemental Material).

4.2.2 The experimental data set

Fig. 4.S.2 shows the result of the preliminary experiment measuring RNA dynamics of the *ADRP* gene with one hour resolution. In our preliminary modelling (see Appendix, Fig. 4.S.1), we found that to discriminate between various models, we would need a higher time resolution. Consequently we next measured a detailed response to ligand treatment at 15-min intervals over a total period of 225 min (Fig. 4.1C,D and Fig. 4.2A,B). The deviation between individual experiments was relatively high (average standard deviation was 20-25% of the mean, but also up to 40% for some time points) especially for pre-mRNA which is less abundant. A possible explanation for this would be a more than single exponential dynamics of the underlying phenomenon with variation of the timing of this between the individual experiments. Because our modelling showed that such faster dynamic behaviour would indeed result from relevant kinetic models (see below), we decided not to throw away the data as 'too noisy', but to analyse them in further detail. The open circles in the figure indicate the averages of the data obtained for each time point and

indeed, some dynamic behaviour. As in Fig. 4.S.2, the first significant induction of the pre-mRNA (Figure 4.1.C) was observed at 30 min. In Fig. 4.2, the overall increase did not seem to be monotonous. The peaks at 45, 120 and 210 min were found to be significant with comparison to the minima at 15, 75 and 150 minutes respectively. This is in line with other studies (Karpova et al., 2008). In contrast, mature RNA (Figure 4.1D) increased only gradually, the first significant increase was detected at 90 minutes with a 60-minute delay compared to the first significant increase in the pre-mRNA. This indicates the occurrence of a delay in mRNA dynamics, which necessitates a model with reaction sequences.

In order to make these numbers amenable to mathematical modelling we expressed the mRNA abundance in terms of number of mRNA molecules per cell. First, we estimated the copy number in an untreated sample from the standard curve of the Ct values versus the copy number (the full description of the procedure can be found in the Appendix section 4.S.2). We then calculated it for the treated samples using the fold induction relative to the untreated sample. The average number of mature RNA copies per gene was around 18, which is approximately 15 times higher than that of the pre-mRNA measured (on average 1.1 copies). The error of the copy number measurements was rather high (Fig. 4.S.3) due to experimental limitations, but the lower estimate of the mature mRNA copy number was still 5 times higher than the higher estimate for the pre-mRNA.

To further enlarge the experimental dataset on transcription dynamics, we measured the decay of mRNA species adding the specific CDK9 inhibitor DRB (5,6-Dichloro-1-β-D-ribofuranosylbenzimidazole) after cells had been treated for 3h with PPARδ ligand. This inhibitor has been shown to prevent promoter escape by the Pol II complex and not to affect elongating polymerases (Yankulov et al., 1995). The decay kinetics were measured as expression levels relative to that of the house-keeping gene (glyceraldehyde-3-phosphate dehydrogenase, *GAPDH*) mRNA, the level of which did not change during 5h of DRB treatment (Fig. 4.S.4), confirming its expected high stability We observed a relatively fast decay of the pre-mRNA on a scale of 10 min after a delay of a few minutes (Fig. 4.2C). This delay we attribute to the production of pre-mRNA by polymerases that already have escaped the promoter but have not yet reached the second exon. In the case of the mature mRNA, we observed a delay of 1 h prior to the start of the degradation (Fig. 4.2D).

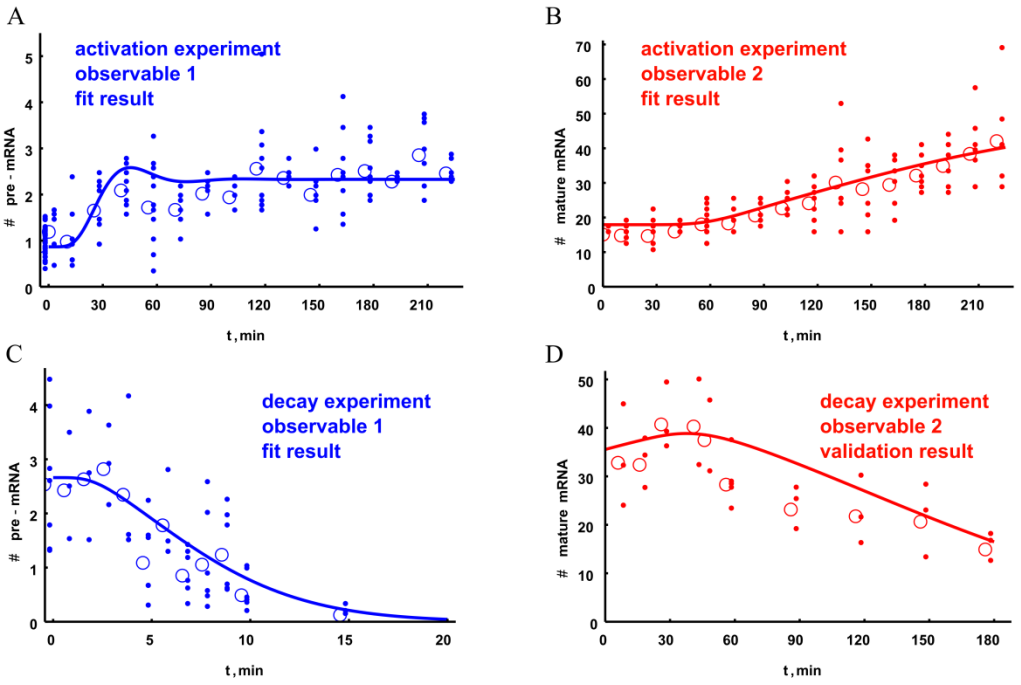

Figure 4.2. Overview of the experimental data and performance of the mathematical model. The dynamic response of the PCR primer pairs marked in blue and red in Figure 1A is shown in Figure A and B, respectively, upon transcription activation of the *ADRP* gene by GW501516. Figure C and D display transcript decay dynamics upon inhibition of transcription initiation by DRB. In all figures, the points indicate individual data points and the circles indicate averaged values at specific time points at 15 min intervals. The lines indicate the performance of the fitted model. The mathematical model of Figure 1B, in its n=5 version (see Table 1 and see supplemental material) was fitted to the data in Figure 2A-C (solid lines) and validated with the data in Figure 2D. Further information about the performance of the mathematical model can be found in the main text and the supplemental information. All the individual data points are reported in Tables S2 and S3 of the supplemental materials. We multiplied the copy numbers of the pre-mRNA decay data by a factor of 0.4 so that the average of the pre-mRNA ligand data at $t = 180$ became equal to the average of the pre-mRNA decay data at $t = 0$, which was not so in the primary data set.

4.2.3 Parameter estimation and validation of the mathematical model

Six mathematical models - five corresponding to Figure 4.1B and one to Fig. 4.S.1 were fitted to the experimental data shown in Figure 4.2A-C. The five multi-step models differed in the number of substates in the 7 states of the

model in Fig. 4.1B were allowed to have (counting initiation and elongation together). The last model had only two states and corresponded to promoter being constantly active. For each of these models the kinetic parameters as well as the initial conditions of the mathematical model were estimated by minimizing a Maximum Likelihood Estimator (MLE), which quantifies the distance between model output and experimental data (see Appendix). We used a global minimization algorithm called Controlled Random Search (Price, 1983), which was modified to enhance performance.

Table 4.S.5 shows the sum of the squares of the differences between the best fit and the experimental data points divided by the number of data points. The number became as low as 0.40, which shows that the fits are satisfactory, which is perhaps surprising because of the noise apparent in the experimental data set (Fig. 4.2). With the exception of the n=0 model (the two state model of Fig. 4.S.1A) the models are not much different in fit quality. This suggests that the transcription dynamics is determined by a multi-state sequential process, but it does not enable us to decide which from these experimental data. We here further focus on the n=5 model because that is of intermediate complexity. In the n=5 model all states of Fig. 1B have 5 substates and the activation by the ligand acts on the first two of the five transitions in the activation state.

Not all parameter values could be estimated equally well from the experimental data. A straightforward assessment of (*a posteriori*) parameter identifiability is the evaluation of the dependency of the estimation objective the Maximum Likelihood Estimate on the parameter values. The optimal parameter set, i.e. the one that best describes the data corresponds to a minimum of the MLE. If the MLE depends strongly on a parameter value then this parameter value is strongly constrained by the data and otherwise not. One of the ways to assess that is to compute the independent and dependent confidence intervals for the parameters (Table 4.2). The calculations for n=5 model indicate that certain parameter values (k_{elo}, k_{spl}, k_{mat}, and k_{deg}) are fairly well constrained as both independent and dependent confidence intervals are similar and relatively small. By contrast, k_{rev}, k_{dea} and k_{ini}, were poorly defined as the independent confidence intervals are much bigger than the dependent ones indicating a strong co-dependence between these parameters (also reflected by the covariance coefficients, Table.4.S.6). The k_{act} was also co-dependent with other promotor constants but less strongly. In Table 4.2, we compare the fitted parameters to their values reported in the literature, and find that the estimated

values lie within ranges measured experimentally by various methods. This is true both for the parameters that are well and for the ones that are poorly constrained by the fitting.

4.2.4 Validation

To validate the mathematical model we compared the simulated and experimental profiles of mature mRNA upon blocking transcription initiation with DRB after 3h of ligand induction (Fig. 4.2D). The overall degradation timescale of the mature mRNA was in the order of several hours and displayed a pronounced delay of about 1 h. This may well reflect the expected influx of pre-mRNA that is still in the process of maturation into the mature mRNA pool. The prediction of mature mRNA decay was very close to the experimentally measured values (Fig. 4.2D).

4.2.4.1 Degradation mechanism

The degradation of mRNA can involve 5' to 3' and/or 3' to 5' degradation pathways. In order to test which of them is involved, we compared the amount of the polyA-containing mRNA detected by either 5' (exon 1) or 3' (exon 6) fragments. In case of primarily 5' to 3' degradation the expectation would be that the amount of exon 6 fragments would be higher, and in case of 5' to 3' the amounts would be equal. The average amounts of the mature mRNA species detected using exon 1,3 and exon 5,6 primers were rather close (18 and 25, respectively) and due to the relatively big error margin of the measurement could be the same (Fig. 4.S.3). Moreover, assuming that there was a difference and the degradation of the exon 6 was slower, a difference in the accumulation dynamics of the exon 1 and exon 6 containing mature mRNA would be expected. However, according to the results of real-time qPCR using primers specific to one of the RNA ends on the template from polyadenylated RNA pool (Fig. 4.S.10B) there was no statistical difference between induction profiles. This allowed us to conclude that the most likely degradation mechanism either involves 3' degradation through deadenylation alone (with subsequent de-capping) or degradation in both directions. As a control confirming that the positioning of the 3' primers does not influence the result of the PCR we designed another primer pair in close proximity to the one used in Fig. 4.S.10A. We did not observe a significant difference between the results from the indicated primer pairs (Fig. 4.S.10C). Furthermore, we tried to

determine the amount of the partially degraded mRNA species. We estimated the copy number of mature mRNA according to exon 5,6 in total mRNA fraction and subtracted the amount found in the polyadenylated fraction. As the pre-mRNA exon 5,6 species are expected to have a relatively short half-life this number would be representative of the partially degraded mRNA species. Surprisingly the estimated number (21) was comparable to that of mature mRNA (Fig.4.S.3), which suggests very low degradation rate of non-functional mRNA. Unfortunately, it proved to be impossible to determine the accumulation dynamics of the partially degraded mRNA due to high experimental error (data not shown).

4.2.4.2 Active promoter state

We further investigated if the model could predict the dynamics of the active promoter state as measured by the presence of the phosphorylated and total polymerase on the *ADRP* gene transcriptional start site (TSS) using ChIP. We observed a significant increase at 30 min perhaps followed by a decrease between 45-60 min, but the latter decrease was not significant statistically (Fig. 4.S.11). The model is qualitatively in agreement with this data to the extent that it predicted the increase of the active promoter state at 30 min (Fig. 4.S.11), although, not the decrease at 60 min (which is expected as the pre-mRNA dynamics in the model do not contain very pronounced oscillations). It is possible, that in the pre-mRNA measurements the oscillatory dynamics is not observed due to biological variability.

4.2.5 Using the mathematical model to detect the site of perturbation

One application of mathematical modelling and parameter estimation that we foresee is the identification of the site of perturbation from comparisons of unperturbed and perturbed mRNA dynamics. To test whether the mathematical model we developed can be used for this purpose, we measured the mRNA dynamics upon gene activation in the presence of a splicing inhibitor. We used the splicing inhibitor isoginkgetin, which targets both the major and minor spliceosomes (O'Brien et al., 2008), but we will here pretend to be ignorant of this information and then see if the model can detect the information in the experimental data. Brief inhibitor treatment (3 h) and co-treatment with PPARδ ligand were insufficient to affect pre- and mature RNA levels (Fig. 4.S.13). Therefore a longer treatment (16 h) with inhibitor was performed which did

have significant effects: it caused increased pre-RNA levels by a factor of 3 (Fig. 4.3C) and the level of mature mRNA decreased slightly below the control case (Fig. 4.3D). The subsequent treatment with the PPARδ ligand caused an increase of the pre-mRNA with a broad peak observed at 75-105 minutes (Fig. 4.3C). The final fold change was smaller compared to the control case, possibly due to non-specific effects of the inhibitor.

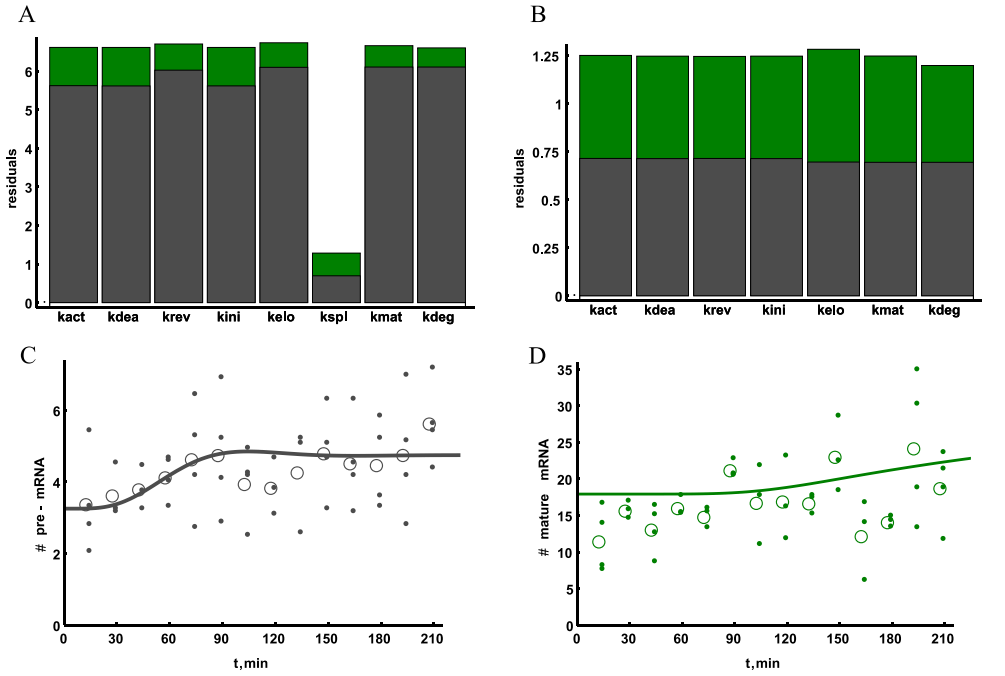

Figure 4.3: Re-fitting the model can indicate the perturbation in the system. Human HepG2 cells were incubated with 100 µM isoginkgetin for 16 h and subsequently treated with PPAR δ ligand GW501516 for the indicated time. Quantitative real-time PCR was performed in order to measure pre- (C) and mature mRNA levels (D) after splicing inhibition. Small filled circles represent all data points from at least four biological experiments corrected for the outliers with MAD method, empty circles the calculated mean. The mathematical model (adjusted for apparent fold induction) was fitted to the data by changing a single constant at a time and the quality of the fit was compared for pre-mRNA (grey) and mature mRNA (green) time courses (A). The best model obtained by lowering the splicing rate constant was further tested for fit improvement by changing the remaining constants. The best fit given by adjusting both splicing and degradation constants is shown for the pre-mRNA (C) and mature mRNA (D) time courses. The mean data points and averaged standard deviations used in the fitting procedure are shown.

We then tried to re-fit the best fitting model (i.e. the one demonstrated in in Figure 4.2) by refitting a single parameter at a time while keeping all other parameters at their original values. The results are shown in Figure 4.3. We then compared the resulting goodness of fit for pre-mRNA and mature mRNA fits. Notably, the only parameter that upon adjustment gave a considerably better fit of the model to the pre-mRNA as well as a better overall fit was $k_{spl,}$ unambiguously pointing to the perturbation of splicing as the action of the added inhibitor (Fig. 4.3C). The resulting splicing constant was around 3 times lower than in the fit of the data in the absence of the added inhibitor, suggesting that the added inhibitor concentration was sufficient to inhibit splicing by some 75%.

We further tested if the fit could be improved further by changing other constants in addition to k_{spl} (Fig. 4.3D). Only a slight improvement could be achieved, and only by increasing k_{deg}, but this was below the level of significance. We conclude that the model successfully predicts the primary site of the applied perturbation, and that it is robust against spurious 'prediction' of other sites.

We analysed if the prediction depended on the particular set of parameters. We changed each parameter independently and compared the effect on the quality of the original model fit and on that of the adjusted model. As shown in Fig.4.S.14 the independent parameter perturbations leading to a decrease in the original fit quality caused a proportional decrease in the adjusted fit.

This was not the case when the similar procedure was to estimate the effect correlated changes of the co-dependent parameters (k_{act}, $k_{dea,}$ k_{ini} or k_{rev}). If the co-dependent constants were changed so that the overall rate of mRNA production stayed the same, the relative decrease in adjusted model fit quality was much lower. This means that worse fitting models could be successfully fitted to the perturbed data. The latter could have been be expected due to poor constrains of promoter constants when changed in a co-dependent manner. This indicates that if the site of perturbation was at the promoter level it would likely be impossible to distinguish between changes in, for example, initiation and promoter deactivation rates.

4.3 Discussion

In this paper we integrated a mathematical modelling and parameter estimation procedure with some targeted experiments, to help understand the dynamics of a nascent mRNA population upon activation of transcription. The model is capable of capturing observed experimental delays in appearance of mature mRNA by explicitly incorporating the essential processes of mRNA transcription and processing. The measurement of transcription dynamics was performed by using carefully chosen PCR primer pairs along the body of the *ADRP* gene. By comparing the transcription dynamics of a reference and perturbed cell line, the model correctly predicted the site of perturbation from the transcription dynamics of the perturbed conditions.

The experimental data we used were quite noisy (Fig. 4.2), due to the difficulty of the experimental techniques used, or perhaps due to systematic experimental variability. Their noisiness would have precluded us from drawing any conclusion. By implementing mathematical models we were able to reach two important conclusions, without being disturbed by the noise: the transcription dynamics reflects a sequential process of more than one step (the n=0 model did not work well), and the applied inhibitor could be identified as acting on slicing. We owe these conclusions to the phenomenon that the making of mathematical models and their fitting can be done in objective ways that stay away from preconceptions. We think that this is an important message of this paper: modelling can enable one to extract information from noisy data. In physics this phenomenon has been appreciated for a long time already. But in biology where many recent cell biological experiments tend to be full of noise, our message may be even more useful.

The transcription parameters (Table 4.2) estimated by fitting the model to the experimental data come close to values reported in the literature. We estimated the promoter cycling time to be around 60 to 70 min (calculated as the sum of three phases of the promoter cycle). This is in agreement with the timescales indicated by the ChIP experiments that measure presence of the TFs on the gene promoters. Several studies found periodic binding of various specific and general TFs in the range of 45 to 90 min (Kang et al., 2002; Metivier et al., 2003; Saramaki et al., 2009). A study in yeast also described oscillation in the mRNA of a copper regulated gene with a period of 50min, which is produced by the synchronous bursts of mRNA production in cells (Karpova et al., 2008).. In our experimental system, although there is evidence for the multi-step

promoter cycle, the oscillations in either mRNA or promoter states were not significant. This could result from relatively irreproducible promoter cycle times or due to too much noise in the data. Recently, time resolved transcriptional activity on a single cell level has been measured for several genes (Suter et al., 2011). The promotor cycle timescales we estimated are within the range found in this study. The available estimation of the initiation time on a eukaryotic promoter based on the in vivo single cell measurement (0.8 min) is also reasonably close to higher of our estimates. As has been shown previously (Chubb et al., 2006) it is not possible to establish the mRNA burst size accurately from the steady state mRNA distributions. Therefore the found range of 5-40 molecules is only suggestive but none the less fits well with the calculated (a ration of characteristic times of the promoter deactivation and initiation) burst size of 12 mRNA molecules.

The estimated Pol II elongation rate in our system was 0.45 kB/min; which is considerably slower than what has been reported for mammalian system, ranging from 1 to 4 kB/min (Singh and Padgett, 2009). On the other hand, Darzacq *et al* found that while the actual elongation rate of a mammalian PolII was 4 kB/min due to pausing the average polymerase progression rate was only 0.4 kB/min (Darzacq et al., 2007), close to our estimation here. With this progression rate it would take the polymerase about 40 min to complete the ADRP transcription, which is less than the observed maturation time of 60 min; the discrepancy might be due to a higher frequency of pausing, to additional time spent on 3' processing or on posttranscriptional splicing of some of the introns. The splicing of the first intron occurs co-transcriptionally as the measured excision rate (~8 min) is much faster than the overall maturation time. The splicing rate that we find is within the range of 5-10 min described by Singh and Padgett for various introns in several human genes (Singh and Padgett, 2009).

The half-life of ~2 h we found for the ADRP mRNA is considerably shorter than the 5h reported previously (Fan et al., 2009b). The reason for the discrepancy may lie in differences between the cell lines used, but may also be a result of the degradation rate fitting procedure that does not take into account any delay due to maturation. If we would fit ADRP mature mRNA degradation with a single exponent the half-life we obtain (~4 h) is much closer to the literature values.

Our results show that it is possible to estimate all the main parameters of the transcription process from a modest data set. We also find that an inhibitor preventing escape of the PolII can be used for simultaneous measurement of the polymerase progression (due to delays caused by elongation), splicing and mRNA degradation rates. On the one hand delays in the mRNA decay data can affect the measured degradation rates if not taken into the account. On the other hand, in many studies in literature such a delay can be found in the mature mRNA decay profiles (Müller et al., 2007; Murray and Schoenberg, 2008; Xu et al., 1998). Therefore, we believe that our approach may well be useful for simultaneous measurement of various mRNA metabolism properties of many genes.

process	equations
activation	$\frac{dx_1^{act}}{dt} = k_{rev} x_{n3}^{rev}(t) - k_{act} x_1^{act}(t)$ ***for i=2:5*** $\frac{dx_i^{act}}{dt} = k_{act} x_{i-1}^{act}(t) - k_{act} x_i^{act}(t)$
deactivation	$\frac{dx_1^{dea}}{dt} = k_{act} x_{n1}^{act}(t) - k_{dea} x_1^{dea}(t)$ ***for i=2:5*** $\frac{dx_i^{dea}}{dt} = k_{dea} x_{i-1}^{dea}(t) - k_{act} x_i^{dea}(t)$
reversion	$\frac{dx_1^{rev}}{dt} = k_{dea} x_{n2}^{dea}(t) - k_{rev} x_1^{rev}(t)$ ***for i=2:5*** $\frac{dx_i^{rev}}{dt} = k_{rev} x_{i-1}^{rev}(t) - k_{rev} x_i^{rev}(t)$
initiation	$\frac{dx_1^{elo}}{dt} = k_{ini} \sum_{i=1}^{n2} x_i^{dea}(t) - k_{elo} x_1^{elo}(t)$
elongation	***for i=2:5*** $\frac{dx_i^{elo}}{dt} = k_{elo} x_{i-1}^{elo}(t) - k_{elo} x_i^{elo}(t)$
splicing	$\frac{dx_1^{spl}}{dt} = k_{elo} x_{n4}^{elo}(t) - k_{elo} x_1^{spl}(t)$ ***for i=2:n5*** $\frac{dx_i^{spl}}{dt} = k_{spl} x_{i-1}^{spl}(t) - k_{spl} x_i^{spl}(t)$
maturation	$\frac{dx_1^{mat}}{dt} = k_{spl} x_5^{spl} - k_{mat} x_1^{mat}$ ***for i=2:5*** $\frac{dx_i^{mat}}{dt} = k_{mat} x_{i-1}^{mat}(t) - k_{mat} x_i^{mat}(t)$
degradation	$\frac{dx_1^{\deg}}{dt} = k_{mat} x_{n6}^{mat}(t) - k_{\deg} x_1^{\deg}(t)$ ***for i=2:5*** $\frac{dx_i^{\deg}}{dt} = k_{\deg} x_{i-1}^{\deg}(t) - k_{\deg} x_i^{\deg}(t)$

Table 4.1: **ODE description of the irreversible multi-step model of mRNA metabolism**. The equations describe model presented in Fig. 4.2B. Activation process corresponds to the induction phase, deactivation – to the active phase and reversion – to the inactive phase of the promotor cycle.

Process	Value of fitted rate constant, min^{-1}	Dependent confidence interval	Independent confidence interval	Characteristic time, min*	Reported range for characteristic time
Activation	0.106	0.0022	0.0498	47.1	10-150 min (Suter et al., 2011)
Deactivation	1.3	0.0256	6.8294	3.8	1-15 min (Suter et al., 2011)
Reversion	1.145	0.2840	4.9264	4.4	N/A
Initiation	3.436	0.0627	18.9286	0.27	0.8 min (Darzacq et al., 2007)
Elongation	2.272 0.45 kB/min**	0.4780	0.7861	2.2	0.38 -4.3 kB/min (Darzacq et al., 2007; Singh and Padgett, 2009)
Splicing	0.512	0.0158	0.0817	9.8	5-10 min (Singh and Padgett, 2009)
Maturation	0.161	0.0337	0.0940	31.1	-
Degradation	0.025	0.0008	0.0047	202.4	30-900 min (~300*** min) (Schwanhausser et al., 2011) (Fan et al., 2009a; Moreira and Holmberg, 1998)

Table 4.2: Overview of the fitted model parameters and comparison to values reported in the literature. * The characteristic times are defined as n/k, with n as the number of elementary steps in the processes (always n=5 except for initiation where n=1). ** The elongation rate in kb/min as calculated from the fitted characteristic time (2.2min) and the length of the amplified fragment (1178nt). *** Degradation rate found specifically for ADRP time mRNA.

4.4 Materials and Methods

Cell culture*:* HepG2 human hepatocellular carcinoma cells were cultured in DMEM medium containing 10% fetal bovine serum (FBS;), 2 mM glutamine and 100 U/ml of a penicillin-streptomycin mixture in a humidified 95% air/ 5% CO_2 incubator. ~24h prior to treatment cells were seeded into medium with 5%fetal bovine serum (FBS) that was treated charcoal in culture flasks containing 10^6 cells. For all experiments cells were treated either with solvent (DMSO at a final concentration of 0.1% W/V or with 100 nM PPAR-delta ligand GW501516 (Alexis Biochemicals, San Diego, CA

RNA extraction and Real-time quantitative PCR*:* Total RNA was extracted from 10^6 using the Quick-RNA^{TM} MiniPrep isolation kit (Zymo) and cDNA synthesis was performed for 60 minutes at 37 ^{O}C using 40 U of M-MuLV reverse transcriptase (Fermentas), 1.0 g of total RNA as a template and 100 pM oligodT_{18} or random hexamers as primers (Fermentas). Real-time quantitative PCR was performed using iCycler (BioRad) and Absolute SYBR Green Fluorescein (Thermo Scientific). The PCR conditions were: pre-incubation for 15 min at 95 ^{O}C, followed by amplification steps of 40 cycles of 30 s at 95^{O}C, 30 s at primer specific temperatures (Supplementary Table 1), 40 s at 72 ^{O}C and a final elongation process of 5 min at 72 ^{O}C.

'Fold induction' (R) was calculated using the formula $2^{-(\Delta\Delta Ct)}$, where $\Delta\Delta Ct$ is the $\Delta Ct_{(ligand)}$-$\Delta Ct_{(DMSO)}$, ΔCt is the $Ct_{(ADRP)}$-$Ct_{(house\ keeping\ gene)}$ and Ct is the cycle number at which the threshold is crossed. Quality of the PCR product was monitored using post-PCR melt curve analysis. The $\Delta Ct_{(ligand)}$-$\Delta Ct_{(DMSO)}$ did not change significantly with duration of DMSO exposure (Fig. 4.S.15)

RNA copy number measurement: DNA fragments were amplified using specific primers (Supplementary Table 1), 'Hot start Taq' (Ferments) and iCycler (BioRad). Products were resolved usin 1.5 % agarose gels and cleaned using QIAEX® II gel extraction kit (Qiagen). The amount of cDNA fragment was measured using the Quant-iT^{TM} PicoGreen® dsDNA Assay Kit (Invitrogen) and the numbers of *ADRP* fragment copies per unit sample volume were calculated. A series of 1/10 dilutions was used to create a standard curve of the Ct value against copy number of the molecules added to reaction (Fig. 4.S.16A-C). A transcript of barnase-coding polyadenylated mRNA was produced from an unmodified pFN19K plasmid and purified by Promega *in vitro* transcription kit. The transcript concentration was measured

by Nanodrop. The transcript was added to the cDNA synthesis reaction in the amounts of 6* 10^7 to 1.5 *10^6 copies and the resulting amount of cDNA was measured according to Ct vs copy number standard curve (Fig. 4.S.16D) to establish the cDNA synthesis efficiency. This standard Ct vs copy number curve was used to calculate the number of copies in DMSO treated cell samples known to have an ADRP Ct close to average . From this, the copy number was calculated in the cDNA solution, mRNA extract and the cell, taking into account the cell number in the culture (counted before seeding; doubling time of the cells much exceeded than the duration of the experiment) and maximal mRNA yield per culture. An example of calculation can be found in the section 4.S.2 in the Appendix.

Chromatin immune recipitation (ChIP) assays: Nuclear proteins were cross-linked to genomic DNA by adding formaldehyde directly to the medium to a final concentration of 1 % for 5 min at room temperature. Cross-linking was stopped by the addition of glycine to a final concentration of 125 mM and a further incubation for 5 min at room temperature. Subsequently, medium was removed, cells were washed twice with ice-cold phosphate-buffered saline (PBS) and collected by scraping. After centrifugation, the pellet was resuspended in lysis buffer (1% SDS, 10 mM EDTA, 50 mM TRIS-HCl pH8, protease inhibitors) and sonicated by a Bioruptor (Diagenode, Liege, Belgium) to result in DNA fragments of 300-1000 bp in length. Cellular debris was removed by centrifugation and the lysates were diluted 1:10 in ChIP dilution buffer (20 mM Tris-HCl pH 8, 2 mM EDTA, 1% Triton X-100, 150 mM NaCl). Chromatin solutions were incubated at 4 ^{O}C with rotation with 5 µg of antibodies against Pol II (sc-899), pPol II S5 (ab5131), or control IgG (sc-2027). The immuno-complexes were collected by adding 60 µl of protein A agarose slurry (Millipore) and incubating for 2 h at 4 ^{O}C with rotation. The beads were collected by centrifugation for 2 min at room temperature at 500 x g and washed subsequently with 1.0 ml of the following buffers: ChIP wash 1 (20 mM Tris-HCl pH 8, 2.0 mM EDTA, 1 % Triton X-100, 150 mM NaCl), ChIP wash 2 (20 mM Tris-HCl pH8, 2.0 mM EDTA, 1 % Triton X-100, 0.1 % SDS, 500 mM NaCl), ChIP wash 3 (0.25 M LiCl, 1 % NP-40, 1 % Na-deoxycholate, 1.0 mM EDTA, 10 mM Tris-HCl of pH8) and finally twice with TE buffer (10 mM Tris-HCl, 1 mM, EDTA, pH8). The immuno-complexes were then eluted by adding 300 µl of elution buffer (1% SDS, 0.1 M $NaHCO_3$) and incubating 30 min at 65 ^{O}C. The supernatant was removed and the beads were washed for 2 min with 200 µl of elution buffer. Supernatants were

combined and proteins were digested overnight at 65 ^{O}C using proteinase K (Fermentas, final concentration = 40 μg/ml). Genomic DNA fragments were recovered by phenol-chloroform extraction and a subsequent ethanol precipitation.

PCR of Chromatin Templates: Genomic primers for the *ADRP* TSS were designed and for their quantification 6-carboxyfluorescein (FAM)-modified probe was used (Supplementary Table 2). Real-time PCR was performed with TaqMan® Universal Master Mix II, no UNG (Applied Biosystems) using the 7500 Fast Real-Time PCR System (Applied Biosystems). The cycling conditions were: pre-incubation for 10 min at 95 ^{O}C, followed by amplification steps: 40 cycles of 15 s at 95 ^{O}C and 1 min at 63 ^{O}C. For the negative region primers were designed (Supplementary Table 2) and real-time PCR was performed with Absolute Blue QPCR SYBR low Rox Mix (Thermo Scientific) using the 7500 Fast Real-Time PCR System (Applied Biosystems). The cycling conditions were: pre-incubation for 15 min at 95 ^{O}C, followed by amplification steps: 40 cycles of 30 s at 95 ^{O}C, 30 s at 60 ^{O}C, 30 s at 72 ^{O}C and final elongation for 10 min at 72 ^{O}C. Relative association of chromatin-bound proteins was calculated using the formula $2^{-(\Delta Ct)}$, where ΔCt is the $Ct_{(output)}$-$Ct_{(input)}$. Output is the immune precipitated DNA and input is the purified DNA from the starting material of the ChIP assay. Fold changes were calculated relative to the control IgG

Splicing inhibition: 0.3 million cells were seeded into medium with low (5%) charcoal-treated fetal bovine serum (FBS) content. The next day Isoginkgetin (kindly provided Dr. Willmar Schwabe GmbH & Co. KG) was added to a final concentration of 50 μM. 16 h later cells were treated either with solvent (DMSO, final concentration=0.1 % W/V) or ligand GW501516 (final concentration=100 nM).

RNA degradation: HepG2 cells were treated either with vehicle (DMSO, final concentration = 0.1 % W/V) or 100 nM GW501516 for 3 h and then new RNA synthesis was blocked by treating the cells with 50 μM DRB (5,6-Dichloro-1-β-D-ribofuranosylbenzimidazole, Sigma).

Modeling and parameter fitting: The general models of mRNA metabolism were implemented and the time courses were simulated in Mathematica 8.0 (Wolfram Research Inc., Mathematica, Version 6.0, Champaign, IL, USA) using standard inbuilt algorithms. The time course data was fitted using a customary algorithm programmed in Matlab. *A posteriori* identification

analysis and additional data fitting was carried out in Mathematica using a Differential Evolution method of the NMinimize algorithm. Details of the system structure parameters and approaches are given in the Appendix.

Appendix 3

4.S.1 Exploration of two models of gene transcription

To illustrate the importance of model choice we compare two alternative models of mRNA dynamics. One model is highly simplified and considers continuous ('constitutive') mRNA production, first-order maturation and first-order degradation (Fig.4.S.1A). It is described by the following equations:

$$\frac{dx^{pre}}{dt} = k_{ini} - k_{mat}x^{pre}(t) \quad (4.S.1a)$$

$$\frac{dx^{mat}}{dt} = k_{mat}x^{pre} - k_{deg}x^{mat} \quad (4.S.1b)$$

Fig. 4.S.1 shows the pre-mRNA (x^{mat}, F-H, dotted) and mature mRNA species (x^{deg}, C-E, dotted).

The second model takes into account a multi-step promoter cycle, mRNA maturation and degradation (Fig. 4.S.1B). Here we explore a general multi-step model which we will make more detailed (including explicitly elongation and splicing) in the subsequent sections for the purposes of data fitting. The systems were described by the following set of equations:

$$\frac{dx_1^{act}}{dt} = k_{dea}x_{n2}^{dea}(t) - k_{act}x_1^{act}(t) \quad (4.S.2a)$$

for i=2:5

$$\frac{dx_i^{act}}{dt} = k_{act}x_{i-1}^{act}(t) - k_{act}x_i^{act}(t)$$

$$\frac{dx_1^{dea}}{dt} = k_{act}x_5^{act}(t) - k_{dea}x_1^{dea}(t) \quad (4.S.2b)$$

for i=2:10

$$\frac{dx_1^{mat}}{dt} = k_{ini}\sum_{i=1}^{5} x_i^{dea}(t) - k_{mat}x_1^{mat}(t) \qquad (4.S.2c)$$

for i=2:15

$$\frac{dx_i^{mat}}{dt} = k_{mat}x_{i-1}^{mat}(t) - k_{mat}x_i^{mat}(t)$$

$$\frac{dx_1^{\deg}}{dt} = k_{mat}x_{15}^{mat}(t) - k_{\deg}x_1^{\deg}(t) \qquad (4.S.2d)$$

for i=2:15

$$\frac{dx_i^{\deg}}{dt} = k_{\deg}x_{i-1}^{\deg}(t) - k_{\deg}x_i^{\deg}(t)$$

The pre-mRNA species plotted in Fig. 4.S.1 (F-H, solid) is defined as $\sum_{i=1}^{15} x^{mat}$, and mature mRNA (Fig. 4.S.1C-E, solid) as $\sum_{i=1}^{15} x^{deg}$. Parameters used for the simulation of the various time courses can be found Table 4.S.1. At the start of the simulation all the variables are 0 except for *i=6:10* $x_i^{dea} = 0.2$.

	Model	k_{act}	k_{dea}	k_{ini}	k_{mat}	k_{deg}
$T_{cyc}>T_{mat}$	a*	0.167	0.500	1.000	1.000	0500
$T_{cyc}>T_{deg}$	b*	-	-	0.146	0.067	0.033
$T_{cyc} > T_{mat}$	a	0.167	0.500	4.000	1.000	0.125
$T_{cyc} <T_{deg}$	b	-	-	0.583	0.067	0.008
$T_{cyc} < T_{mat}$	a	0.167	0.500	1.000	0.200	0.125
$T_{cyc} <T_{deg}$	b	-	-	0.146	0.013	0.008

Table 4.S.1: Parameter values used for alternative mRNA metabolism models simulation presented in Fig. 4.S.1.a – simplified single step model, b – multi-step model for promoter cycle, maturation and degradation.

In Fig. 4.S.1C-H the time courses of the pre-mRNA and mature mRNA abundance are shown upon gene activation. The rate constants were adjusted so

that the overall production, maturation and degradation rates and starting/ending steady state values of the mature mRNA are the same. Notably, for the multi-step model the dynamics vary significantly depending on the parameter regime, i.e. the relative rates of promoter cycling, mRNA maturation and degradation, but are always distinct from those of the simplified single step model. If degradation and maturation occur fast compared to the promoter cycling both the mRNA and the pre-mRNA accumulation displays damped oscillatory dynamics for the more complicated model (Fig. 4.S.1C,F). This is explained by the fact that simultaneously activated cells go through a round of mRNA production leading to a rise and then, during promoter silent period, part of the pre-mRNA is spliced, and part of mature mRNA is degraded resulting in a decrease (Fig. 4.S.1C). Then the promoter is active again, producing an increase in mRNA and so on. In the single step model, on the other hand, the parameter regimes only affect the accumulation rate but not the overall form of the profile; in all cases both the pre-mRNA and mature mRNA increase monotonously without damped oscillations (Fig. 4.S.1 C-H).

4.S.2 Data analysis

We have data from two time course experiments: ligand activation of transcription and inhibition of transcription initiation (degradation time course). From both experiments at each time point the pre-mature and mature mRNA Ct values are available, as well as the Ct-value of a housekeeping gene. The Ct-values are converted to expression levels and to copy numbers as demonstrated below.

Let C_m be the Ct value of the RNA under investigation, C_H the Ct of the RNA of the house keeping gene that does not change expression during the experiment and $M = C_m - C_H$. We define the expression level 'E' by $E = 2^{-M}$ which is the expression level relative to that of house-keeping (baseline) gene. This procedure corrects for the technical variation due to sample preparation. For each data point at t>0 we acquire an M (and a corresponding E) value of the experimental (ligand or inhibitor treated) sample. It is then corrected by the average M of the control samples ($\bar{M}_{cntr}$) belonging to the particular repeat of the experiment, giving $dM = M - \bar{M}_{cntr}$. The fold induction R over control treatment is defined as 2^{-dM}. This procedure corrects for the biological variation (different cell culture) between the experiments. Only dM (and R)

values can be compared between the experiments but not C_m or M values. However, to estimate the copy number from the standard curve a C_m value is required. Thus the C_m's are calculated back using average M and C_H of all the control samples: $C'_m = dM - \bar{M}_{cntr} - \overline{C_H}$. In case of t=0 (or control samples) the calculation is $C'_m = M - \overline{C_H}$.The copy number should be given by:

$$\text{t=0: } a \cdot 10^{\frac{b-(M-\overline{C_H})}{c}}$$

$$\text{t>0: } a \cdot 10^{\frac{b-(M-\overline{M}_{cntr}-\overline{C_H})}{c}}$$

where *a, b*, and *c* are component-dependent experimental constants, and the bar indicates the mean value. The *b* (the Ct value if the copy number equals 1 in the calibration experiment) and *c* (the exponential factor in the PCR, theoretically equal to $-^2\log 10 = -3.32$) values come from a calibration experiment that establishes relationship between the Ct-value and copynumber in the cDNA sample (Fig. 4.S.16). They allow finding the number of the respective molecule in the sample. Factor *a* is then used to obtain copynumber per cell as it is a product of multiplication of the sample dilution factor (2500 for mature mRNA, 625 for pre-mRNA), the inverse cDNA synthesis efficiency coefficient (1 for mature and 0.1 for pre-mRNA) and the inverse of the cell number in the culture (10^6 cells per culture dish).

These factors are a = 0.00125, b = 38.70, c = -3.69 for mature mRNA (b and c are based on the average fit of the two calibration experiments of Fig. 4.S.16B) and a = 0.003125, b = 38.92, c = -3.70 (based on average fit of the calibration experiment in Fig. 4.S.16A) for pre-mRNA time courses.

For the ligand activation experiment we have 17 time-points for both pre-mature and mature mRNA, t^l=(0, 5, 15, (15), 225); for the degradation experiment we have for the pre-mature mRNA 12 time-points, $t^{d,pR}$= (0, (1), 10, 15) and for the mature mRNA 11 time-points, $t^{d,mR}$= (0, 10, 20, 30, 45, 50, 60, 90, 120, 150, 180). All time-points consist of several data points (2-13), for the initial state (t=0) in the ligand activation experiment there are around 45 data points (See the column 'n' in Table 4.S.2).

In our fitting procedure we use the copy number data (see Tables 4.S2-3). We discuss three sources of error in the data.

Device error: The error resulting from the measurement device.

For each datapoint the Ct values measured are an average over 3 measurements.

We have neglected this error as relatively small – the average standard deviation is 0.13 which would result in ±0.1 copynumber error for pre-mRNA and ±1.5 copynumber error for mature mRNA. For comparison the average standard deviation between replicas of a single timepoint in the ligand induction time course is 0.52 for pre-mRNA and 5.8 for mature mRNA.

Conversion error: The error resulting from the conversion from C t-values to copy numbers. The copy number of pre-mRNA at t = 180 should be equal to the copy number of the starting value in the decay experiment for the pre-mRNA measurements. This was not the case in the primary data, for an unknown reason. We have corrected for this by multiplying the copy numbers of the pre-mRNA decay data by a factor (0.3998) such that the average of the pre-mRNA ligand data at t = 180 became equal to the average of the pre-mRNA decay data at t = 0 of that experiment. With this corrected pre-mRNA decay data we fit our model and we have assumed further conversion errors to be negligible.

Sample error: The error resulting from the variation over cells. We assume the error in the copy-number to be independent for each measurement and to be normally distributed per time point.

Plots of all time courses are presented in Fig. 4.2A-C. In view of the substantial noise, the number of data points per time point is too small to use the mean+sd as fit data. 'Averaging' the standard deviation over more time points is questionable since for some data courses (mature mRNA ligand and pre-mRNA degradation) the hypothesis of no correlation between time points is clearly rejected (Pearson correlation between time point and standard deviation for the mature mRNA ligand is 0.72 and for pre-mRNA degradation -0.78). Therefore we use all data-points in a Least Square Estimation fitting procedure which is a standard procedure for the fitting of overdetermined systems. Assuming a scaled constant standard deviation for all timepoint error distributions this results in a Maximum Likelihood Estimate. For the scaling we used a factor of 10 for the mature mRNA results as there is approximately one order of magnitude difference between the mean values of pre-mRNA and mature mRNA.

t	Premature mRNA	n
0	1.03 1.07 1.19 1.27 0.71 0.63 0.93 0.80 1.32 0.79 0.89 0.84	
	1.03 1.20 1.52 0.46 1.55 0.92 0.94 1.11 1.18 1.07 0.91 1.02 0.89	
	1.21 0.63 0.72 0.59 0.95 1.59 1.02 1.17 1.21 1.29 1.30	
	1.23 1.37 1.35	39
5	1.73 1.73 1.53 0.53 0.99	5
15	1.64 2.45 0.65 1.1 0.53 0.65 0.99	7
30	0.99 2.54 1.42 0.99 2.35 1.53 2.15 2.15 2.25	9
45	2.35 2.74 1.94 2.85 2.54 2.15 1.84 1.64	8
60	2.45 2.25 1.10 0.76 3.33 1.73 1.84 0.41 2.64 2.74 1.84 1.50	12
75	2.05 2.25 1.10 1.53 1.94 1.73 2.25	7
90	2.15 2.54 1.64 2.25 2.35	5
105	2.05 1.73 2.05 2.25 2.45	5
120	3.43 2.64 1.73 1.84 1.94 1.84 2.85 3.14 3.43 5.11 2.05	11
135	2.25 2.54 2.45 2.85 2.54	5
150	2.05 2.35 2.25 1.32 1.94 3.05	6
165	1.64 2.45 2.15 3.52 2.85 1.42 2.54 4.19	8
180	1.94 3.22 3.22 2.05 3.52 2.05 2.64 3.33 2.45 2.35	10
195	2.45 2.35 2.45 2.54	4
210	3.72 2.74 1.94 2.25 3.81 3.63 3.05	7
225	2.85 2.54 2.35 2.45 2.94	5
N = 17		154

t	Mature mRNA	n
0	15.35 13.55 17.18 12.24 15.13 17.68 15.84 16.48 21.50 13.75 15.29 16.48 13.55 14.36 19.22 12.01 14.13 17.00 15.74 15.42 18.55 12.92 14.42 18.90 30.37 12.52 15.77 20.08 31.60 13.52 17.07 18.98 27.95 12.86 12.26 18.32 32.46 12.21 12.16 12.21 16.04 17.39 23.18 30.95 24.67 23.86 24.11 25.13 33.14	49
5	16.76 16.76 18.40	3
15	15.07 20.09 16.76 13.39 16.76 15.07 20.09 18.4 16.76 16.76 16.76 18.40	12
30	18.40 16.76 16.76 11.60 13.39 13.39 23.33 20.09 18.40 16.76	10
45	16.76 20.09 18.40 20.09 16.76 16.76 18.40	7
60	23.33 26.43 24.99 18.40 16.76 13.39 16.76 26.43 13.39 21.65 20.09 21.65 20.09	13
75	20.09 26.43 23.33 16.76 20.09 16.76 20.09	7
90	26.43 21.65 26.43 21.65 20.09 18.40 24.99	7
105	28.13 21.65 31.28 21.65 21.65 23.33 26.43	7
120	20.09 28.13 26.43 20.09 23.33 16.76 32.88 32.88 32.88 26.43 29.76	11
135	40.4 37.49 53.83 26.43 16.76 26.43 24.99	7
150	34.35 35.88 43.54 35.88 16.76 21.65 24.99	7
165	34.35 37.49 20.09 31.28 24.99 34.35 38.92	7
180	35.88 38.92 32.88 32.88 28.13 29.76 35.88 35.88 41.94 31.28	10
195	41.94 41.94 44.92 29.76 28.13 34.35 38.92	7
210	40.4 46.64 58.38 29.76 41.94 37.49 29.76	7
225	41.94 49.33 69.96 41.94 29.76 32.88	6
N = 17		177

Table 4.S.2: The ligand activation induced RNA abundance primary data (copy numbers) of the experiment reported in Fig. 4.1B,C(pre-mature RNA=observable 1) and Fig. 4.2B (mature m-RNA=observable 2) of the main text. The data are here in terms of copy numbers, calculated as described in section “data analysis”. Time t is in minutes. n refers to the number of replica data points at the same time point, N to the number of time points examined.

t	pre-mature mRNA							n
0	4.61	3.44	3.50	6.66	10.10	11.34	7.22	7
1	8.89	6.41	3.98					3
2	7.02	9.86	3.93					3
3	5.55	7.45	9.22					3
4	3.93	4.17	10.57					3
5	1.82	0.98	1.82	4.03	5.75	4.14		6
6	3.87	7.17	3.29					3
N = 12								56
t	mature mRNA							n
0	38.80	30.87	51.24	36.38	35.77	28.39	46.54	7
10	29.01	41.79	25.25					3
20	33.94	32.10	29.01					3
30	35.16	35.16	47.72					3
45	31.49	48.31						2
50	30.25	44.18						2
60	29.63	22.07	36.98	27.77	36.38			5
N = 11								37

Table 4.S.3: RNA abundance primary data of the inhibitor induced decay experiment of the experiment reported in Fig. 4.2C (pre-mature RNA=observable 1) and Fig. 4.2D (mature m-RNA=observable 2) of the main text. The data are here in terms of copy numbers.

4.S.3 Mathematical models

In the ligand activation experiment the system is assumed to be initially in steady state. Let f be the ratio between the steady state value of pre-mature mRNA species in the steady states after and before the ligand addition. f is experimentally determined from the ratio of the average of 2-3 replicates of 5 late time points (t=240, 255, 270, 285 and 300min) and the average of all the

datapoints at t=0 (Table 4.S.2). For pre-mRNA the average at t>4h is found to be 3.1 copies per cell, resulting in f of 2.96 and for mature mRNA the respective average is 44.6 copies per cell and f of 2.42. The average $\boldsymbol{f}$ subsequently used is 2.69.

4.S.3.1 Model n=0

The simplest model (see Fig. 4.S.1A) is given by the following equations:

$$\frac{dx^{mat}(t)}{dt} = u_{ini} \cdot k_{ini} - k_{mat} \cdot x^{mat}(t) \qquad (4.S.3a)$$

$$\frac{dx^{deg}(t)}{dt} = k_{mat} \cdot x^{mat}(t) - k_{deg} \cdot x^{deg}(t) \qquad (4.S.3b)$$

For the ligand activation experiment the input variable u_{ini} = 1, for the degradation experiment, where initiation was stopped abruptly by addition of an inhibitor of initiation, u_{ini} = 0.

4.S.3.1.1 Solutions

For this simple system a closed solution still gives insight, the pre-mature mRNA is a simple exponential function and the mature mRNA a combination of two exponentials.

$$x^{mat}(t) = \left(x^{mat}(0) - \frac{u_{ini} \cdot k_{ini}}{k_{mat}}\right) e^{-k_{mat} \cdot t} + \frac{u_{ini} \cdot k_{ini}}{k_{mat}} \qquad (4.S.4a)$$

$$x^{deg}(t) = \left(x^{deg}(0) - \frac{k_{mat} \cdot x^{mat}(0) - u_{ini} \cdot k_{ini}}{k_{mat} - k_{deg}} - \frac{u_{ini} \cdot k_{ini}}{k_{deg}}\right) e^{-k_{deg} \cdot t} \cdot k_{deg} + \frac{k_{mat} \cdot x^{mat}(0) - u_{ini} \cdot k_{ini}}{k_{mat} - k_{deg}} e^{-k_{mat} \cdot t} + \frac{u_{ini} \cdot k_{ini}}{k_{deg}} \qquad (4.S.4b).$$

4.S.3.1.2 Initial conditions

In the ligand activation experiment the system is assumed to be initially in steady state, but it is the steady state condition without ligand addition. Since we assume ligand addition to influence only k_{ini} the steady state before ligand addition should correspond to the solution of (4.S.1a) with k_{ini} replaced by k_{ini} /f . For the degradation experiment the initial states are unknown and have to be fitted to the data. So the initial conditions are given by the following equations:

$$x^{mat}(0) = \frac{u_{ini} \cdot k_{ini}/f}{k_{mat}} + (1 - u_{ini}) x_0^{mat} \qquad (4.S.5a)$$

$$x^{deg}(0) = \frac{u_{ini} \cdot k_{mat} \cdot x_0^{mat}}{k_{deg}} + (1 - u_{ini}) x_0^{deg} \qquad (4.S.5b)$$

Where x_0^{mat} is an unknown parameter, x_0^{deg}=38.28 is the mean of the experimental data values at t=0 for the decay experiment (Fig. 4.2D) and *f*=2.69.

4.S.3.2 Multi-step model, n=1,3,5,10,20

The multi-step model (see Fig. 4.S.2B) differentiates in the promoter cycle between activation, deactivation, reversion, and initiation, and in the maturation between elongation, splicing, and maturation. It is given by the following equations.

activation

$$\frac{dx_1^{act}}{dt} = k_{rev} x_{n3}^{rev}(t) - k_{act} x_1^{act}(t) \qquad (4.S.6a)$$

for i=2:n1

$$\frac{dx_i^{act}}{dt} = k_{act} x_{i-1}^{act}(t) - k_{act} x_i^{act}(t)$$

deactivation

$$\frac{dx_1^{dea}}{dt} = k_{act} x_{n1}^{act}(t) - k_{dea} x_1^{dea}(t) \qquad (4.S.6b)$$

for i=2:n2

$$\frac{dx_i^{dea}}{dt} = k_{dea} x_{i-1}^{dea}(t) - k_{dea} x_i^{dea}(t)$$

reversion

$$\frac{dx_1^{rev}}{dt} = k_{dea} x_{n2}^{dea}(t) - k_{rev} x_1^{rev}(t) \qquad (4.S.6c)$$

for i=2:n3

$$\frac{dx_i^{rev}}{dt} = k_{rev}x_{i-1}^{rev}(t) - k_{rev}x_i^{rev}(t)$$

initiation

$$\frac{dx_1^{elo}}{dt} = k_{ini}\sum_{i=1}^{n2} x_i^{dea}(t) - k_{elo}x_1^{elo}(t) \quad (4.S.6d)$$

elongation

for i=2:n4 (4.S.6e)

$$\frac{dx_i^{elo}}{dt} = k_{elo}x_{i-1}^{elo}(t) - k_{elo}x_i^{elo}(t)$$

splicing

$$\frac{dx_1^{spl}}{dt} = k_{elo}x_{n4}^{elo}(t) - k_{elo}x_1^{spl}(t) \quad (4.S.6f)$$

for i=2:n5

$$\frac{dx_i^{spl}}{dt} = k_{spl}x_{i-1}^{spl}(t) - k_{spl}x_i^{spl}(t)$$

maturation

$$\frac{dx_1^{mat}}{dt} = k_{spl}x_{n5}^{spl}(t) - k_{mat}x_1^{mat}(t) \quad (4.S.6g)$$

for i=2:n6

$$\frac{dx_i^{mat}}{dt} = k_{mat}x_{i-1}^{mat}(t) - k_{mat}x_i^{mat}(t)$$

degradation

$$\frac{dx_1^{\deg}}{dt} = k_{mat}x_{n6}^{mat}(t) - k_{\deg}x_1^{\deg}(t) \quad (4.S.6h)$$

for i=2:n7

$$\frac{dx_i^{\deg}}{dt} = k_{\deg}\cdot x_{i-1}^{\deg}(t) - k_{\deg}\cdot x_i^{\deg}(t)$$

4.S.3.2.1 Solution

Also this system of equations has a closed solution. Because we do not find it insightful, we omit this and use numerical solutions only.

4.S.3.2.2 Initial conditions

In the ligand activation experiment the initial state of the system is the steady state before ligand addition. The addition of the ligand is assumed to only have an effect on the first $n1^0$ steps of the activation process (see Fig. 4.1). The basal level of the activating transcription factor is lower in these first steps (hence $k_{act}^0 < k_{act}$); if the ligand is added it reaches approximately the same level as the transcription factor for the second part of the activation. To reach an f -times higher 'production' from the promoter cycle, the cycle time should be f times as fast, giving the following relationship between the activation rate constants before (k_{act}^0) and after (k_{act}) the ligand addition:

$$f\left(\frac{n1}{k_{act}}+\frac{n2}{k_{dea}}+\frac{n3}{k_{rev}}\right)=\left(\frac{n1^o}{k_{act^0}}+\frac{n1-n1^o}{k_{act}}+\frac{n2}{k_{dea}}+\frac{n3}{k_{rev}}\right) \qquad (4.S.7)$$

The initial conditions for system (4.S.6) are then given by the steady-state values of system (4.S.6) with the activation equations (4.S.6a) replaced by

$$\frac{dx_1^{act}}{dt}=k_{rev}x_{n3}^{rev}(t)-k_{act^0}x_1^{act}(t)$$

$$i=2\ldots n1^0 \qquad (4.S.8a)$$

$$\frac{dx_i^{act}}{dt}=k_{act^0}x_{i-1}^{act}(t)-k_{act^0}x_i^{act}(t)$$

$$\frac{dx_{n1^0+1}^{act}}{dt}=k_{act^0}x_{n1^0}^{act}(t)-k_{act}x_{n1^0+1}^{act}(t)$$

$$i=n1^0+2\ldots n1 \qquad (4.S.8b)$$

$$\frac{dx_i^{act}}{dt}=k_{act}x_{i-1}^{act}(t)-k_{act}x_i^{act}(t)$$

Note that if $n1 = n1^0$ all corresponding k_{act} in (4.S.6b) should also be replaced by k_{act}^0.

The system is singular because of the promoter cycle. Therefore one of the 'internal' equations, e.g. the first one above, may be replaced by the mass

conservation relation

$$\sum_{i=1}^{n1} x_i^{act} + \sum_{i=1}^{n2} x_i^{dea} + \sum_{i=1}^{n3} x_i^{rev} = 1 \qquad (4.S.9)$$

Let us denote these steady-state values by x_{*ss}^{*}. Note that system (4.S.6) with its equation for activation replaced by (4.S.9) has to be solved for each new parameter vector in the search procedure.

We have used the following initial conditions for system (4.S.6)

$$x_i^{act}(0) = u_{ini} x_{i\ ss0}^{act} \qquad i=1...n1 \qquad (4.S.10a)$$

$$x_i^{dea}(0) = u_{ini} x_{i\ ss0}^{dea} \qquad i=1...n2 \qquad (4.S.10b)$$

$$x_i^{rev}(0) = u_{ini} x_{i\ ss0}^{rev} \qquad i=1...n3 \qquad (4.S.10c)$$

$$x_i^{elo}(0) = u_{ini} x_{i\ ss0}^{elo} + (1 - u_{ini}) \frac{k_{spl} x_0^{spl}}{k_{elo} n5} \qquad i=1...n4 \qquad (4.S.10d)$$

$$x_i^{spl}(0) = u_{ini} x_{i\ ss0}^{spl} + (1 - u_{ini}) \frac{x_0^{spl}}{n5} \qquad i=1...n5 \qquad (4.S.10e)$$

$$x_i^{mat}(0) = u_{ini} x_{i\ ss0}^{mat} \qquad i=1...n6 \qquad (4.S.10f)$$

$$x_i^{deg}(0) = u_{ini} x_{i\ ss0}^{deg} + (1 - u_{ini}) \frac{x_0^{deg}}{n7} \qquad i=1...n7 \qquad (4.S.10g)$$

with u_{ini} defined as above.

The value $x^{spl}{}_0$ is an unknown parameter to be fitted to the data, and $x^{deg}{}_0$ =38.28 is the mean of the experimental data values at *t = 0* for the decay experiment.

4.S.3.2.3 The variety of multi-step models examined

In this paper we consider the following multi-step models

n=1: $n_1 = n_2 = n_3 = n_4 = n_5 = n_6 = n_7 = 1$, $n_1{}^0 = 1$

n=3 $n_1 = 3$, $n_2 = n_3 = 1$, $n_4 = n_5 = n_6 = n_7 = 5$, $n1^0 = 1$

n=5: $n_1 = n_2 = n_3 = n_4 = n_5 = n_6 = n_7 = 1$, $n_1^0 = 2$

n=10: $n_1 = n_2 = n_3 = n_4 = n_5 = n_6 = n_7 = 1$, $n_1^0 = 4$

n=20: $n_1 = n_2 = n_3 = n_4 = n_5 = n_6 = n_7 = 1$, $n_1^0 = 8$

4.S.4 Fit procedure

We shall use the two time courses for the ligand activation and the time course for the pre-mature mRNA degradation to obtain the unknown parameters in our models. The mature mRNA degradation data will be employed for validation.

4.S.4.1 Model parameters

The parameter vector *p* to be fitted with the three time courses (pre-mature and mature mRNA from the ligand activation and pre-mature mRNA from the degradation experiment) is for the simple model (n = 0) given by

$$p_S = (k_{ini}, k_{mat}, k_{deg}, x_0^{mat}) \tag{4.S.11}$$

and for the multi-step model (n = 1, 3, 5, 10, 20)

$$p_M = (k_{act}, k_{dea}, k_{rev}, k_{ini}, k_{elo}, k_{spl}, k_{mat}, k_{deg}, x_0^{spl}) \tag{4.S.12}$$

The initial guesses for the parameter search are based on the rough manual fit of the experimental data. They are given by

$$p_S = (\frac{1}{10}, \frac{1}{50}, \frac{1}{120}, 2.68) \tag{4.S.13}$$

and

$$p_M = (\frac{n1}{35}, \frac{n2}{10}, \frac{n3}{15}, 1, \frac{n4}{5}, \frac{n5}{10}, \frac{n6}{20}, \frac{n7}{120}, 2.68) \tag{4.S.14}$$

The initial guesses are then used to define the boundaries of the search domain used in the fitting procedure which uses multiple initial parameter vectors. These search boundaries are $[\frac{k}{4}, 4k\ ]$ for any kinetic constant k, and $[\frac{2x_0}{3}, \frac{4x_0}{3}]$ for any initial concentrations x_0.

4.S.4.2 Model observables

We denote the observables by (o^{pR} (t, p, u_{ini}), o^{mR} (t, p, u_{ini})) for the pre-mature mRNA and the mature mRNA respectively. For the simple (n=0) model (Eq.(4.S.3a,b)) the model observables are

$$o^{pR}(t,p,u_{ini}) = x^{spl}(t,p_m,u_{ini}) \quad (4.S.15a)$$

$$o^{mR}(t,p,u_{ini}) = x^{deg}(t,p_m,u_{ini}) \quad (4.S.15b)$$

and for the multi-step model (Eq.(4.S.4ag))

$$o^{pR}(t,p,u_{ini}) = \sum_{i=1}^{n5} x^{spl}(t,p_m,u_{ini}) \quad (4.S.16a)$$

$$o^{mR}(t,p,u_{ini}) = \sum_{i=1}^{n7} x^{deg}(t,p_m,u_{ini}) \quad (4.S.16b)$$

4.S.4.3 Object function

The distance measures per data-set are

$$V^{l,pR}(p) = \sum_{i=1}^{N^l} \sum_{j=1}^{n_i^{l,pR}} (o^{pR}\left(t_i^l,p,1\right) - ed^{l,pR}(t_i^l,j))^2 \quad (4.S.17a)$$

$$V^{l,mR}(p) = \sum_{i=1}^{N^s} \sum_{j=1}^{n_i^{l,mR}} (\frac{o^{mR}\left(t_i^l,p,1\right) - ed^{l,mR}(t_i^l,j)}{10})^2 \quad (4.S.17b)$$

$$V^{d,pR}(p) = \sum_{i=1}^{N^d} \sum_{j=1}^{n_i^{d,pR}} (o^{pR}\left(t_i^d,p,0\right) - ed^{d,pR}(t_i^d,j))^2 \quad (4.S.17c)$$

$$V^{d,mR}(p) = \sum_{i=1}^{N^d} \sum_{j=1}^{n_i^{d,mR}} (\frac{o^{mR}\left(t_i^d,p,0\right) - ed^{d,mR}(t_i^d,j)}{10})^2 \quad (4.S.17d)$$

where N denotes the number of time-points, *n* the number of data-points per time-point, and *ed* the experimental data; the upper-indices stand for *l*-ligand addition experiment, *d*-degradation experiment, *pR*-pre-mature mRNA, *mR*-

mature mRNA. The object function we use for the fit procedure is

$$V(p) = V^{l,pR}(p) + V^{l,mR}(p) + V^{d,pR}(p) \qquad (4.S.18)$$

The first part (4.S.17a) compares the model with the pre-mature mRNA data of the ligand activation experiment, the second part (4.S.17b) with the mature mRNA data of the ligand activation experiment, the third part (4.S.17c) with the pre-mature mRNA of the degradation experiment. (4.S.17d) will be used to evaluate the quality of the validation with mature mRNA decay time course and is not included in the objective for the fitting therefore. We have scaled the two 'mature' terms with 10 to take the difference of the concentration values into account. Note that the parameter vector *p* for which this object function V is minimal is a Least Squares Estimate; for it to be a Maximum Likelihood Estimate (Draper and Smith, 1988) same variance of the relative error distributions of the data in all time points is assumed.

4.S.4.4 Search

We employed a standard global search algorithm, called Controlled Random Search (CRS) (Price, 1977). The main idea behind this algorithm is that, starting with an initial collection of parameter vectors, CRS repeatedly draws a new parameter vector that replaces a vector in the collection if its data fit is better. The CRS method starts with taking a random set of n_Q parameter vectors inside a search domain D by drawing random values from the uniform distribution (confined by *D)* for each parameter value for each vector. Then the corresponding values of the object function are computed for each vector in the set. The bounds of D represent the *a priori* limits for the parameters.

From this list of n_Q vectors, a new vector is created using the rule

$$p_{new} = 2\overline{p}_{rand} - p_{rand}, \qquad (4.S.19)$$

where p_{rand} is a random vector from the domain, and $\overline{p}_{rand}$ is the average of a random subset of p vectors in the domain. To ensure that the new vectors are selected with equal preference over the logarithmic space, equation (4.S.19) is modified element wise to

$$p_{new} = 10^{\log(2\overline{p}_{rand}) - \log(p_{rand})}. \qquad (4.S.20)$$

If $V(p_{new}) < \max(V(p))$, and $p_{new} \in D$, the parameter vector with the highest object function is replaced by the new one:

$$p \mid \{S(p) = \max(S(p))\} \rightarrow p_{new}. \tag{4.S.21}$$

By repeating this, the worst fitting parameter vectors are removed continuously and replaced by ones with a better fit. Eventually, the points will form a cloud that gets denser and denser. The algorithm stops when

$$\max(S(p)) \leq s_C \cdot \min(S(p)),$$

with s_c the stop criterion. So the worst fit in the remaining collection has an at most $100(s_C - 1)$ % larger S value than that of the best fit. We used the following values: s_c=1.01, n_Q=300. The frequence with which a parameter value was found in new parameter vectors during the fitting is shown in Fig.4.S.6.The resulting optimal parameters are shown in Table 4.S.4.

model	k_{act}	k_{dea}	k_{rev}	k_{ini}	k_{elo}	k_{spl}	k_{mat}	k_{deg}	x_0^{spl}
n=0	-	-	-	0.1887	-	-	0.0797	0.0038	2.5959
n=1	0.0087	0.0251	0.1220	1.7523	0.3906	0.1699	0.0221	0.0087	2.7640
n=3	0.0382	0.0260	0.2153	0.8114	2.8624	0.5034	0.4122	0.0260	2.7585
n=5	0.1061	1.3034	1.1455	3.4361	2.2717	0.5116	0.1607	0.0247	2.6614
n=10	0.6509	2.0463	2.5940	1.1386	3.2848	0.9878	0.2382	0.0473	2.4357
n=20	1.2009	6.9756	5.0111	1.7545	7.7699	1.8565	0.5549	0.0875	2.5040

Table 4.S.4: Best fitting parameters for the models n=0, n=1, n=3, n=5, n=10, n=20.

4.S.5 Statistical and sensitivity analysis

4.S.5.1 Residual analysis

The first step in our *a posteriori* analysis is based on the residual values only. With this we can test whether we should reject the hypothesis that our mathematical model with the obtained parameter vector p^ is an acceptable

description of the data.

There are two types of residual test:

Size-based Here we test the probability that the obtained V($\hat{p}$) lies in the χ^2 distribution corresponding to our number of data-points and number of unknown parameters: χ^2 -test Tχ2 = V($\hat{p}$)∈χ^2(df). If the test value T>δ(α), the hypothesis is rejected. The δ is the value such that cumulative distribution function CDF (χ^2(df))=1−α, with α the confidence level and df the degrees of freedom. The df is defined as df=N-m, where N is the number of datapoints fitted and *m* - the number of parameters under assumption that the parameters are independent.

Correlation-based Here the probability is tested that the residuals are uncorrelated: runs-test $T_{run} = \frac{R_u - N/2}{\sqrt{N/2}} \in N(0,1)$, where R_u is a function of sign changes in V($\hat{p}$) Again if the test value T>δ(α), the hypothesis is rejected.

For all models 95% χ^2 -tests are passed, all fail the 95 % Run-test (both described above) (the interval for 5% confidence interval is (-1.96,1.96)).

model	$V(\hat{p})/N$	$V^{l,pR}(\hat{p})/\Lambda$	$V^{l,mR}(\hat{p})/N^{l,mR}$	$V^{d,pR}(\hat{p})/N^{d,p}$	run-test
n=0	0.49	0.42	0.45	0.78	-7.22
n=1	0.42	0.36	0.39	0.70	-6.87
n=3	0.43	0.40	0.38	0.70	-6.36
n=5	0.44	0.41	0.38	0.70	-6.51
n=10	0.44	0.42	0.38	0.73	-6.79
n=20	0.44	0.42	0.38	0.72	-6.36

Table 4.S.5: Results of the residual analysis for models n=0-20.

Since all of the models have the similar properties according to the statistical tests we can try to discriminate according to the value of the object function – smaller value means better overall fit. Additionally, smaller run-test values are also preferable. Keeping this in mind the better models seem to be n=3, n=5 and n=20, although the differences between all model expect n>0 are not dramatic.

4.S.5.2 Sensitivity analysis n=5 model

For local analysis the pairwise covariance coefficient of the parameters (Table 4.S.6) was calculated. First the sensitivity matrix J was determined by perturbing each parameter by -0.01% in both directions and calculating the corresponding sensitivity coefficient of $V(\hat{p})$ at each datapoint, resulting in 396x8 matrix. The covariance matrix is computed as $cov = (J^T J)^{-1}$and the correlation coefficient between i-th and j-th parameter as $cov_{ij} = \frac{cov_{ij}}{\sqrt{cov_{ii} cov_{jj}}}$.

Further, parameter dependent and independent 95% confidence intervals were calculated (Table 3.2 main text). For global independent parameter sensitivity analysis, parameters were sampled one at a time from a uniform distribution with limits four times lower and higher than the best fit value. This resulted in N=3000 new parameter vectors with single parameter perturbed. Then for each new parameter vector fold change of the object function compared the best fit was calculated. The results are plotted in Fig. 4.S.7.

	k_act	k_dea	k_rev	k_ini	k_elo	k_spl	k_mat	k_deg
k_act	1.000	0.925	0.818	0.942	0.087	0.106	0.168	0.004
k_dea	0.925	1.000	0.737	0.998	0.089	0.078	0.167	0.005
k_rev	0.818	0.737	1.000	0.771	0.076	0.063	0.236	0.071
k_ini	0.942	0.998	0.771	1.000	0.112	0.108	0.194	0.018
k_elo	0.087	0.089	0.076	0.112	1.000	0.789	0.548	0.724
k_spl	0.106	0.078	0.063	0.108	0.789	1.000	0.695	0.918
k_mat	0.168	0.167	0.236	0.194	0.548	0.695	1.000	0.459
k_deg	0.004	0.005	0.071	0.018	0.724	0.918	0.459	1.000

Table 4.S.6: Pairwise covariance coefficients of the parameters in the n=5 model

Additionally, the co-dependent parameter analysis was done sampling the three out of four co-dependent promoter activity rate constants (k_{act}, k_{ini} and k_{rev}) from respective uniform distributions. The ranges were as follows: $0.033^{-6}min^{-1}$ for k_{ini}, $0.025^{-5}min^{-1}$ for k_{act} and k_{rev}. The fourth constant (k_{dea}) was adjusted to keep the mRNA production rate at a fixed value determined by the following relationship:

$$\frac{k_{act}\,k_{rev}\,k_{ini}}{k_{act}\;k_{dea}+k_{act}\;k_{rev}+k_{rev}\;k_{dea}} = v_{mRNA\;prod} \qquad (4.S.20)$$

The rate of mRNA production found in the fitted model was 0.238. With exception of cases when k_{act} deviated from the found by fitting by high percentage values the resulting fits were very close to the original fit (90% of fits have deviation less than 10% of the original).

4.S.6 Validation of the n=5 model

To validate the n=5 model the model output was compared to the mature mRNA decay data (Table 4.S.2). Since the mRNA decay was measured after 180 min of ligand treatment and addition of the inhibitor results in inhibition of initiation at the TSS the following initial conditions were used:

$$x_i^{act}(0) = 0 \qquad i=1...n1 \qquad (4.S.21a)$$

$$x_i^{act}(0) = 0 \qquad i=1...n2 \qquad (4.S.21b)$$

$$x_i^{rev}(0) = 0 \qquad i=1...n3 \qquad (4.S.21c)$$

$$x_i^{elo}(0) = x_i^{elo}(180) \qquad i=1...n4 \qquad (4.S.21d)$$

$$x_i^{spl}(0) = x_i^{spl}(180) \qquad i=1...n5 \qquad (4.S.21e)$$

$$x_i^{mat}(0) = x_i^{mat}(180) \qquad i=1...n6 \qquad (4.S.21g)$$

where the $x_i^n(180)$ is the value of the x_i^n after 180 min of ligand addition. The promoter variables are set to zero as initiation has been inhibited. Since the inhibitor used does not affect polymerases that have escaped the promoter all the mRNA species are still present after the addition of the inhibitor. The value of the resulting object function $V^{d,mR}(\hat{p})/N^{d,mR}$ was 0.43 which is comparable to that of the model fit.

Global analysis of the independent parameter sensitivity of the validation fit was carried in the same manner as the model fit (see 4.S.5.5.2). The results indicate that the validation has same sensitivity as the model fit with exception of being insensitive to k_{spl} value (Fig. 4.S.8).

4.S.7 Refitting the ligand induction time-course after splicing inhibition

The additional data after splicing inhibition was treated in the same way as the other datasets (Table 4.S.7).

t	pre-mRNA				n
0	3.02	3.96	2.73	3.82	4
15	2.88	3.39	2.13	5.5	4
30	4.6	3.24	3.32		3
45	3.32	4.53	3.82		3
60	4.1	4.67	3.39	4.74	4
75	4.25	5.36	2.8	6.51	4
90	4.17	5.29	2.95	6.98	4
105	4.25	4.32	2.58	5.01	4
120	3.89	3.17	4.74		3
135	5.15	2.65	5.29		3
150	4.74	6.38	3.32	5.15	4
165	4.25	6.38	3.24	4.6	4
180	3.68	5.29	3.39	5.91	4
195	5.22	2.88	4.25	7.05	4
210	4.46	5.7	5.5	7.25	4
N=16					56

t	mature mRNA				n
0	13.57	11.27	17.49	21.59	4
15	7.96	8.49	17.01	14.27	4
30	17.3	16.13	14.96		3
45	12.98	9.01	16.72	15.45	4
60	18.07	15.74	15.64		3
75	15.84	13.67	16.33		3
90	20.84	21.03	23.1		3
105	11.37	18.07	22.16		3
120	12.17	23.47	16.52		3
135	18.07	15.55	17.78		3
150	22.82	28.92	18.74		3
165	14.37	6.47	17.1		3
180	13.77	15.25	14.66		3
195	13.67	19.12	35.25	30.56	4
210	12.07	23.94	21.69	19.12	4
N=16					50

Table 4.S.8: RNA abundance data after splicing inhibition (copy numbers)

For re-fitting the model the induction factor f was adjusted to the experimentally observed 1.42 value calculated as the mean of the last five pre-mRNA data points (150-180 min; the mature mRNA does not reach a steady state level in the duration of the experiment). The same observables were used as in the original fitting procedure. The distance measures per dataset were:

$$V^{s,pR}(p) = \sum_{i=1}^{N^s} \sum_{j=1}^{n_i^{s,pR}} (o^{pR}(t_i^s, p, 1) - ed^{s,pR}(t_i^s, j))^2 \qquad (4.S.22a)$$

$$V^{s,mR}(p) = \sum_{i=1}^{N^s} \sum_{j=1}^{n_i^{s,mR}} \left(\frac{o^{mR}(t_i^s, p, 1) - ed^{s,mR}(t_i^s, j)}{5}\right)^2 \qquad (4.S.22b)$$

The object function was defined as sum of the distance measures:

$$V^s(p) = V^{s,pR}(p) + V^{s,mR}(p) \quad (4.S.23)$$

Each single parameter was allowed to change within 4-fold of its original value and the model was fitted anew to the perturbed dataset (Table 4.S.9).

In the second round (run 2) in Table 4.S.9 the changed k_{spl} (which produced the best fit in run1) was inserted into the model and the model was fitted varying each of the remaining rate constants by 4-fold. The list of the factors by which constants were adjusted and of the object function values is presented in Table 4.S.9.

	k_{act}	k_{dea}	k_{rev}	k_{ini}	k_{elo}	k_{spl}	k_{mat}	k_{deg}
$V^s(\hat{p})/N^s$ run 1	6.62	6.61	6.70	6.61	6.74	1.28	6.66	6.60
a run 1	1.1411	0.8872	4.0000	1.1232	4.0000	0.2660	0.2500	1.1734
$V^s(\hat{p})/N^s$ run 2	1.25	1.25	1.25	1.25	1.28		1.25	1.20
a run 2	0.9518	1.0490	0.3526	0.9545	0.6552		0.3255	1.1328

Table 4.S.9: Object functions and parameter adjustment factor for data re-fitting after splicing inhibition. $V^s(\hat{p})/N^s$ is the object function divided by the number of data points, *a* is the raio between the new parameter and the old one.

The sensitivity of the refit to the individual constants perturbations performed same way as in *a posteriori* analysis (see 4.S.5.5.2) of the original model is presented in Fig. 4.S.9.

Finally, the dependence of the prediction quality on the specific parameter values was tested. All but adjusted parameters were sampled independently according to the same procedure as for the parameter sensitivity analysis in the section 4.S.5.5.2. Then for each new parameter vector the fold changes of object function compared to the optimal parameter vector were calculated for both (the original and perturbed) models. The relationship between fold change in the object function of the original model and the perturbed one is plotted Fig. 4.S.14 (blue). Same type of sensitivity analysis was done by sampling co-

dependent promoter activity rate parameters (k_{act}, $k_{dea,}$ k_{ini} and k_{rev}) according to procedure in section 4.S.5.5.2 (Fig. 4.S.14, violet).

Gene fragment	Sequence
mature RNA 5' F	GCA-GTC-CGT-CGA-TTT-CTT-TC
mature RNA 5' R	ACC-GTT-CTC-TGC-CAT-CTC-AC
mature RNA 3' F	GTA-GAA-CAG-TAC-CTC-CCT-CTC
mature RNA 3' R	CGT-GAC-TCA-ATG-TGC-TCA-G
mature RNA 3'ctrl F	CAG-TGA-CTG-GCA-GTG-TGG-AG
mature RNA 3'ctrl R	ACG-GGA-GTG-AAG-CTT-GGT-AG
pre-mRNA F	TGG-AGA-GCT-GGA-GAG-AGG-AA
pre-mRNA R	GTT-GTG-GAT-CAA-CTG-CAA-CG

Table 4.S.10: PCR primer pairs for real-time quantitative PCR**.** The annealing temperature in all cases was 60 ^{O}C. mature RNA 5' primers correspond to red, mature RNA 3' to black, mature RNA 3'ctrl to green and pre-mRNA to blue primers in Fig. 4.S.2 and Fig. 4.S.10**.**

TaqMan probe	Sequence
***ADRP* TSS (FAM)**	CGA-AGA-CGA-CTC-CGG-CTG-CCA-CG
Gene fragment	**Sequence**
***ADRP* TSS F**	ACA-CTC-GGG-CTT-GGG-ACA
***ADRP* TSS R**	GAC-GGA-CTG-CAG-CGA-AAG
NEGATIVE F	GAT-TTT-CCC-CTC-TCC-CTC-TG
NEGATIVE R	TTA-TGC-CAG-GAG-TGC-AAT-GA

Table 4.S.11: Genomic PCR primers sequences and FAM-modified quantitative PCR probe used in ChIP assays

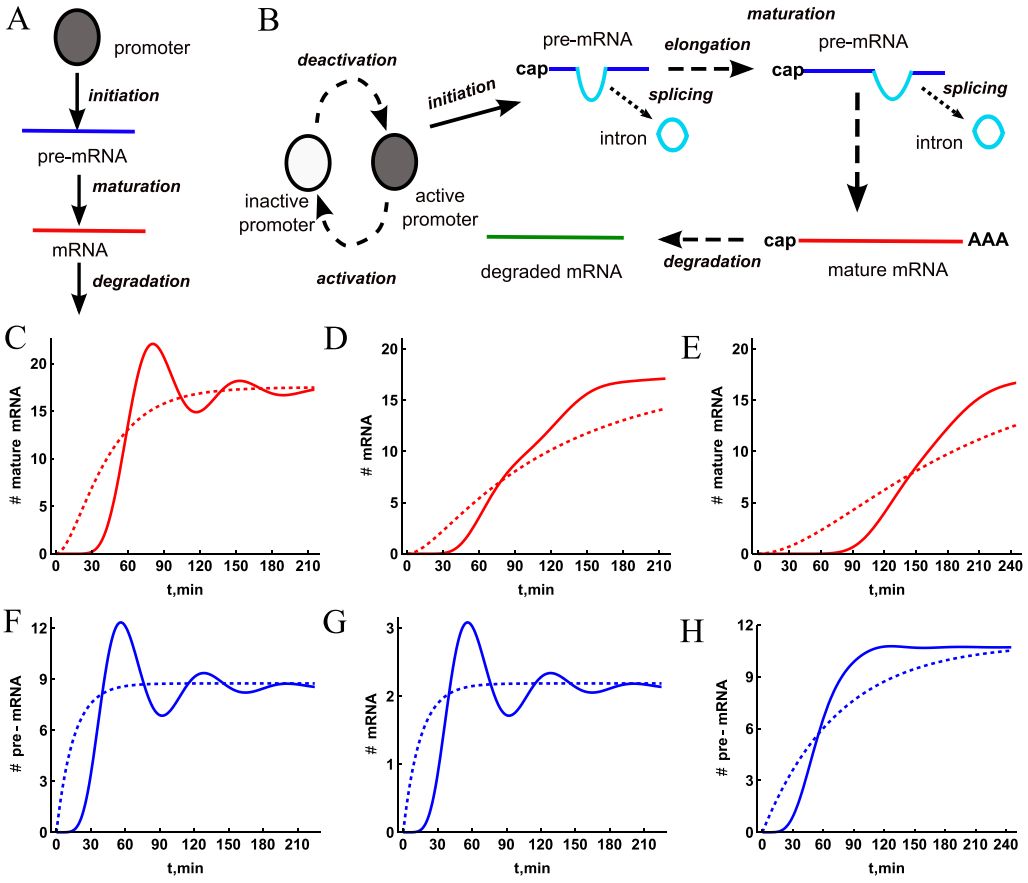

Figure 4.S.1: Alternative models of mRNA dynamics. A highly simplified model of a constitutively active promotor and first-order mRNA elongation and degradation process. (B) A more realistic model that takes into account the promoter cycle, as well as the multi-step nature of mRNA maturation (including elongation and splicing) and degradation. The promoter cycle, maturation and degradation were each taken to have an arbitrary number of 15 irreversible reactions with equal rates. The plots below show mature- (C-E) and pre- (F-H) mRNA induction time courses for the two different models (solid line – refined model B, dotted line – simplified model A) under various parameter regimes: (C, F) when promoter cycling time (T_{cyc}) exceeds the degradation time (T_{deg}) and maturation time (T_{mat}), (D, G) when $T_{cyc} < T_{deg}$ and $T_{cyc} > T_{mat}$, and (E, H when $T_{cyc} < T_{deg}$ and $T_{cyc} < T_{mat}$. All models start with initial conditions corresponding to zero transcription activity (promoter inactive) and have same final steady state for mature mRNA.

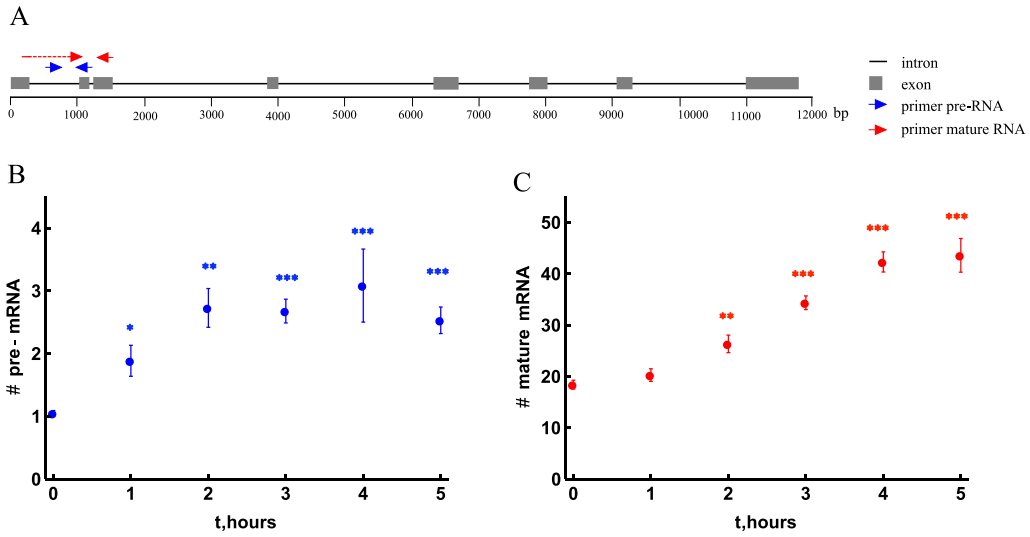

Figure 4.S.2 Upregulation of the *ADRP* gene upon PPARδ ligand treatment. (A) *ADRP* gene primer localization relative to the introns (lines) and exons (boxes). The indicated primers were used in quantitative real-time PCR reactions in order to measure changes in pre- (B; blue primer pair) and mature (C; red primer pair) *ADRP* RNA levels upon 100 nM GW501516 treatment. The data is presented in copy numbers (calculated as described in 4.S.2); housekeeping gene 36B and DMSO control were used as reference values. Data points indicate the means of at least three independent experiments corrected for the outliers with the MAD method. Error bars represent the standard error of the mean. Two-tailed (type 3), paired Student's t-tests were performed to determine the significance of the ligand-dependent regulation of *ADRP* RNA in reference to vehicle (DMSO). *:$p<0.05$, **:$p<0.01$, ***:$p<0.001$

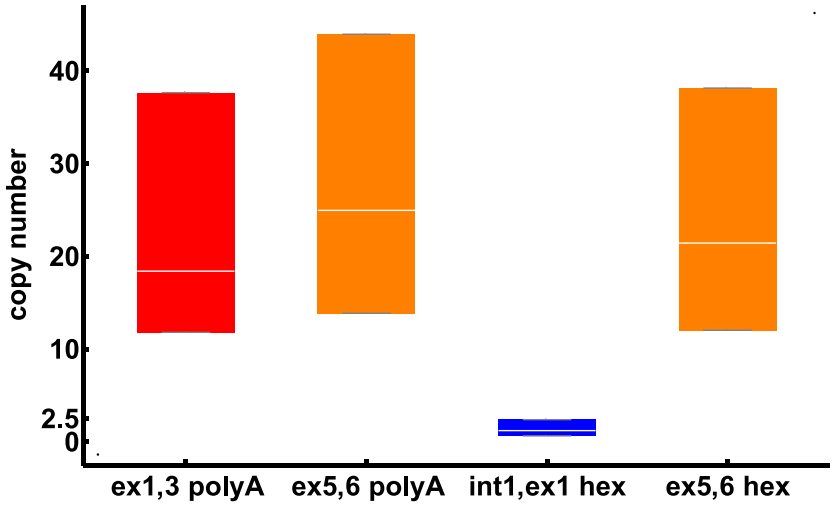

Figure 4.S.3: Copy numbers of different mRNA species per gene copy. Averages are shown as horizontal lines (based on the fitting all the points in Fig.4.S.16 plots) and the maximum-minimum estimation range (based on the blue and red data fits in Fig.4.S.16, respectively) is indicated by the bar. Species containing exon 5,6 border (polyadenylated and non-polyadenylated fractions) are depicted in orange, species containing exon1,3 border (polyadenylated fraction) – in red intron1,exon2 species (total fraction) – in blue.

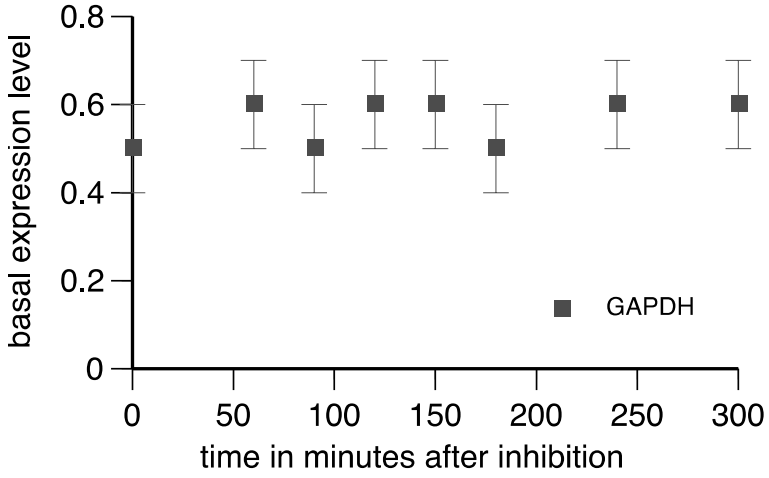

Figure 4.S.4: Measuring *GAPDH* degradation rates. HepG2 cells were treated with 100 nM GW501516 for 3h and then new mRNA synthesis was blocked by treating the cells with 50 μM DRB (5,6-Dichlorobenzimidazole 1-β-D-ribofuranoside). Real-time quantitative PCR was performed in order to measure levels of mature RNA of the *GAPDH* gene relative to house-keeping gene (E). The plot shows that no significant degradation of GAPDH mRNA occurs during the experiment.

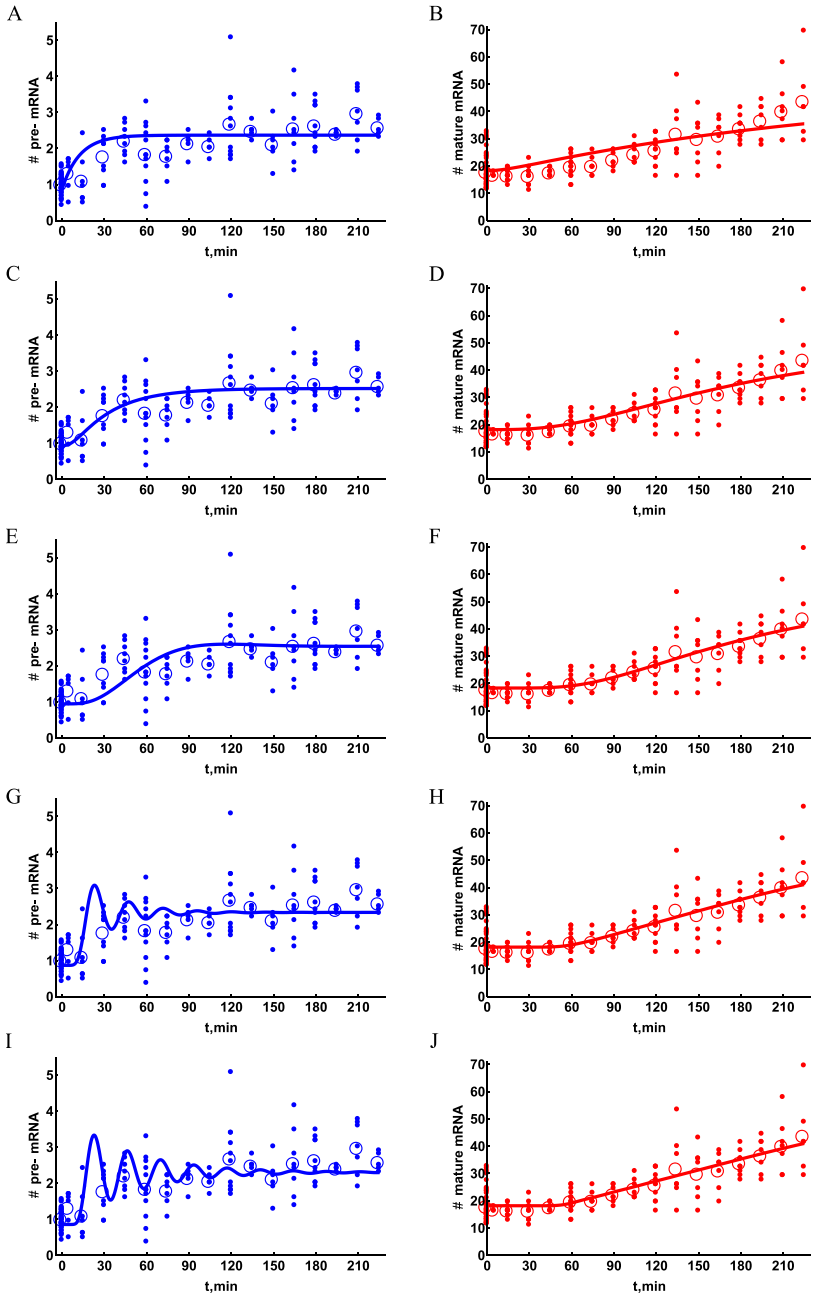

Figure 4.S.5: The fitted mRNA induction time course data for four different models: n=0 (A,B), n=1 (C,D), n=3 (E,F), n=10 (G,H), and n=20 (I,J). The time course for pre-mRNA is shown on the left, for the mature mRNA – on the right. The

fit for the n=5 model can be found in the main text Fig.4.2. Small filled circles present all data points used for fitting, empty circles represent the calculated mean.

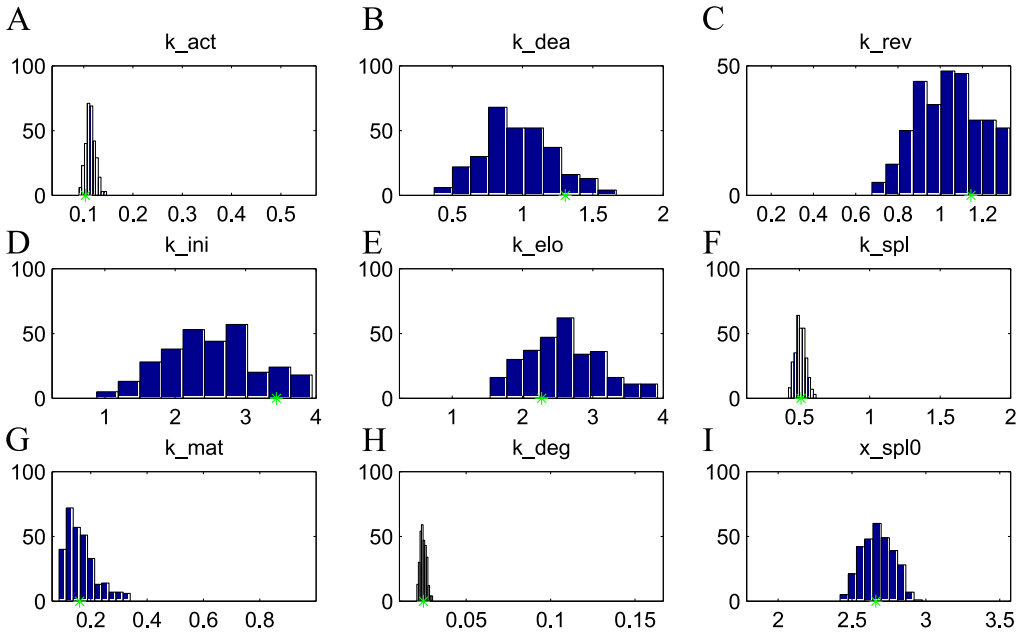

Figure 4.S.6: The parameter values explored in the fitting procedure of the n=5 model. During the fitting procedure new parameter vectors are created according to the following rule $p_{new} = 10^{\log(2\,\bar{p}_{rand}) - \log(p_{rand})}$. where $\bar{p}_{rand}$ is the average of all initial vectors created by drawing from uniform random distributions. How often a certain a certain parameter value is visited is described by distributions plotted for all rate constants (A-H) and for pre-mRNA decay initial conditions (J). The green star indicates the optimal value of the parameter.

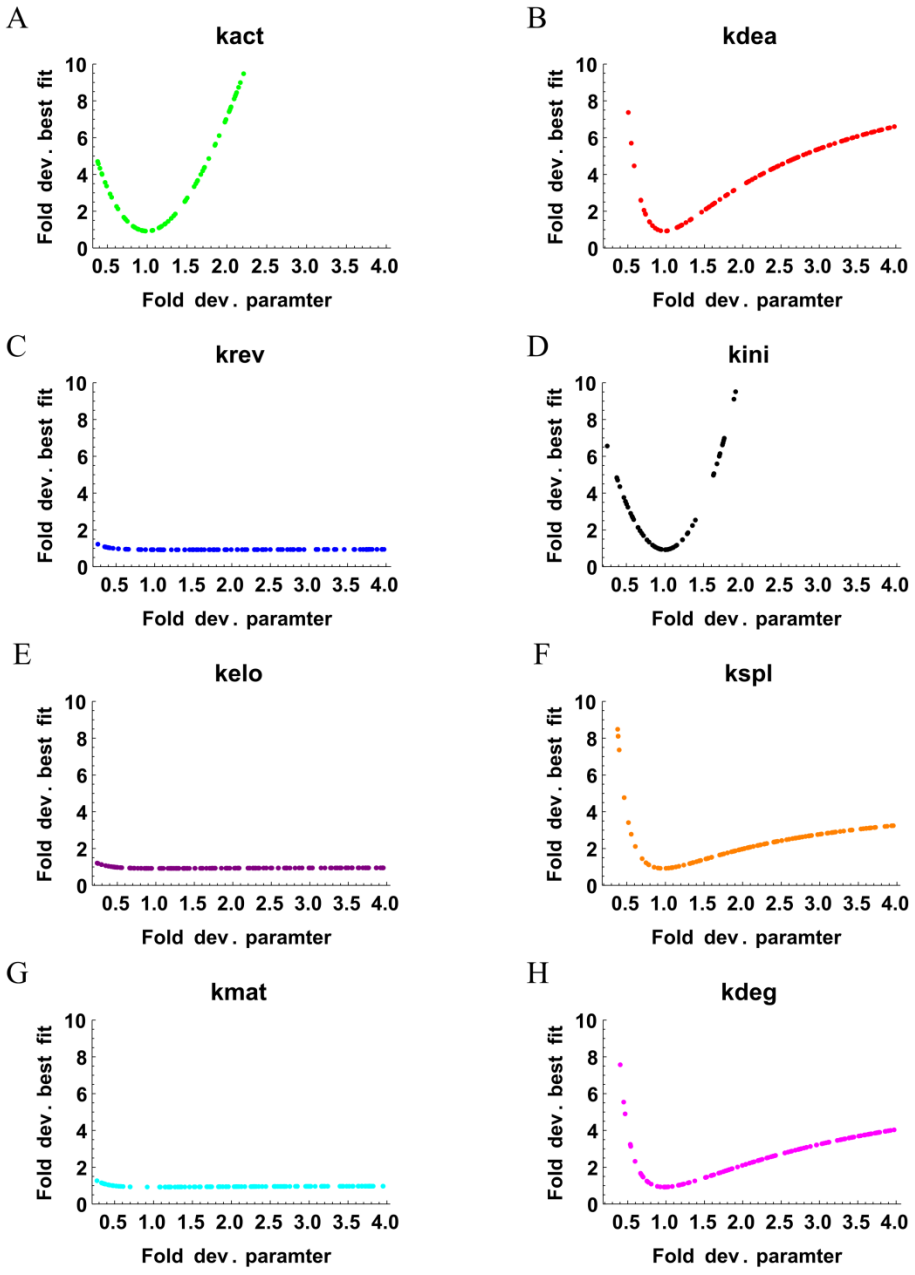

Figure 4.S.7: ***A posteriori*** **analysis of the model n=5 fit sensitivity to the independent parameter perturbation.** The fold deviation of the object function from the best fit $V(\hat{p}_i)/V(\hat{p}_i^{pr})$ (where $\hat{p}_i$ is the perturbed parameter) is plotted against the fold deviation of the parameter perturbation $\frac{\hat{p}_i}{\hat{p}_i^{pr}}$.

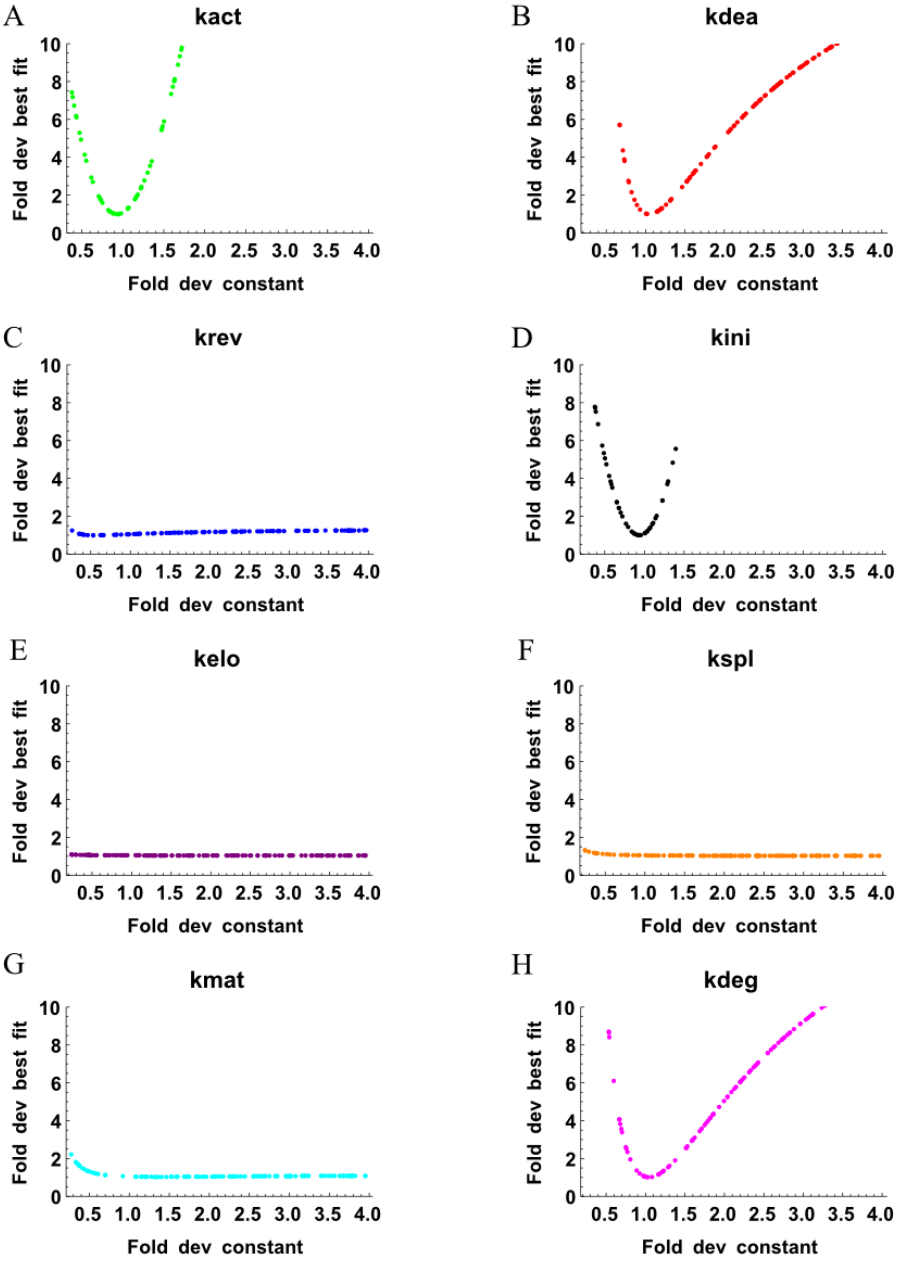

Figure 4.S.8:Analysis of the model validation fit sensitivity to the independent parameter perturbation. The fold deviation of the object function from the best fit $V(\hat{p}_i)/V(\hat{p}_i^{pr})$ (where $\hat{p}_i$ is the perturbed parameter) is plotted against the fold deviation of the parameter perturbation $\frac{\hat{p}_i}{\hat{p}_i^{pr}}$.

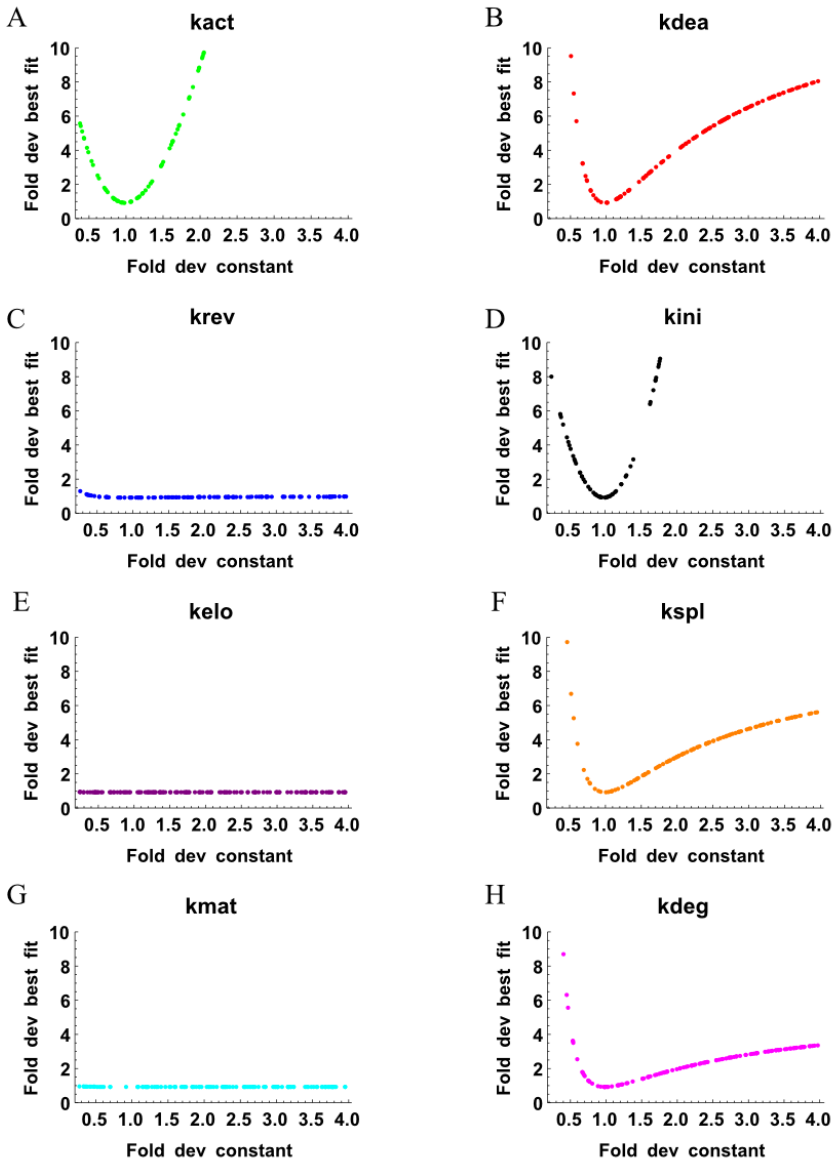

Figure 4.S.9: Analysis of the model refit (after splicing inhibition) sensitivity to the independent parameter perturbation The fold deviation of the object function from the best fit $V(\hat{p}_i)/V(\hat{p}_i^{pr})$ (where $\hat{p}_i$ is the perturbed parameter) is plotted against the fold deviation of the parameter perturbation $\frac{\hat{p}_i}{\hat{p}_i^{pr}}$.

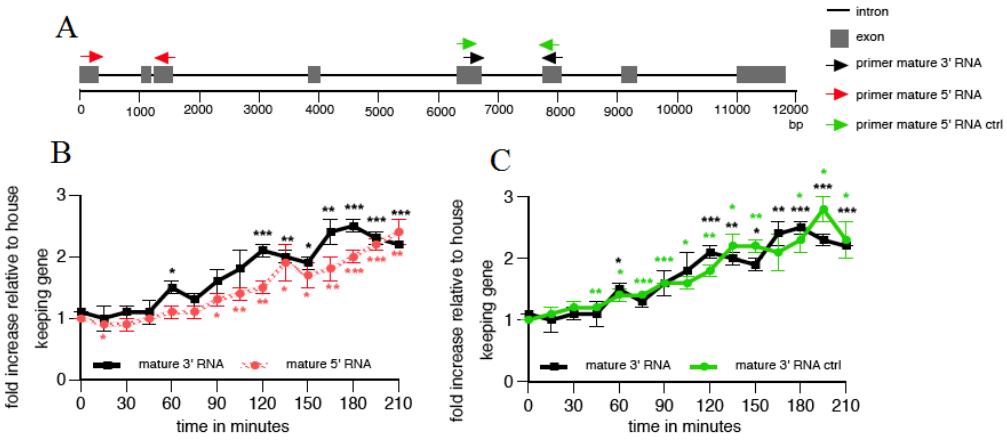

Figure 4.S.10: Estimation of a degradation mechanism and primer set validation. Human HepG2 cells were stimulated with 100 nM GW501516, total RNA was collected and PCR reaction was performed using the polyadenylated RNA fraction as template. A. Primer localization relative to the introns (lines) and exons (boxes) of the human *ADRP* gene. B. In order to determine 5' degradation, primers located in exons 1,3 (red) were used in real-time quantitative PCR. Results were then compared with PCR with primers located in exons 5,6 (black). C. results of a control experiment with both primer sets in exons 5 and 6. Data is presented in terms of fold induction (R) over vehicle (DMSO) treatment. Each data point represent the means of at least three biological replicate samples corrected for the outliers with MAD method, error bars represent the standard error of the mean. Two-tailed, paired Student's t-tests were performed to determine the significance of the ligand-dependent regulation of *ADRP* RNA in reference to vehicle: *p<0.05, **p<0.01, ***p<0.001.

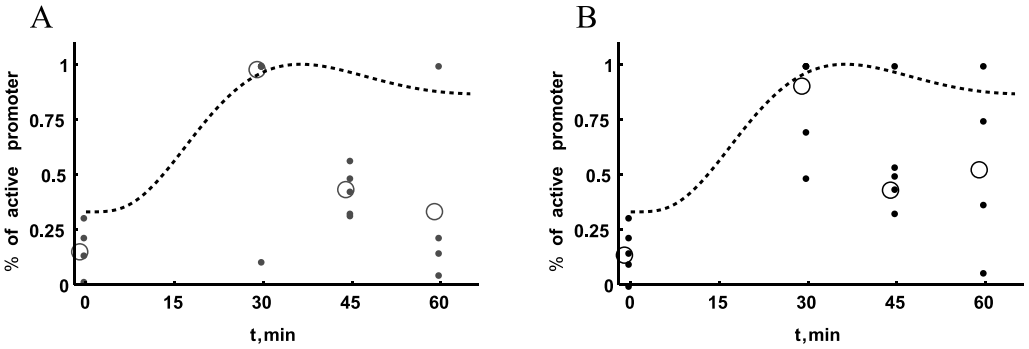

Figure 4.S.11: Comparison of the predicted dynamics of the 'active promoter state' and the experimentally determined presence of the PolII on the *ADRP* promoter. Dashed line: the time course of active promoter state upon induction as predicted by the n=5 model. A chromatin immune precipitation (ChIP) assay with antibodies against Pol II (A) or pPol II S5 (B) was performed on chromatin extracts from HepG2 cells treated with GW501516 for the indicated times. Analyses were performed by real-time PCR with primers listed in Table 4.S.2. For each repeat the enrichment was calculated as a percent of input rescued with indicated antibody relative to percent input rescued with IgG control. The data was rescaled with respect to maximum fold induction – small filled circles represent individual results (individual datapoints with same values may overlap), empty big circles represent the average of all repeats at that time point. The separate repeats and data for negative regions (background binding control) are shown in Fig. 4.S.12.

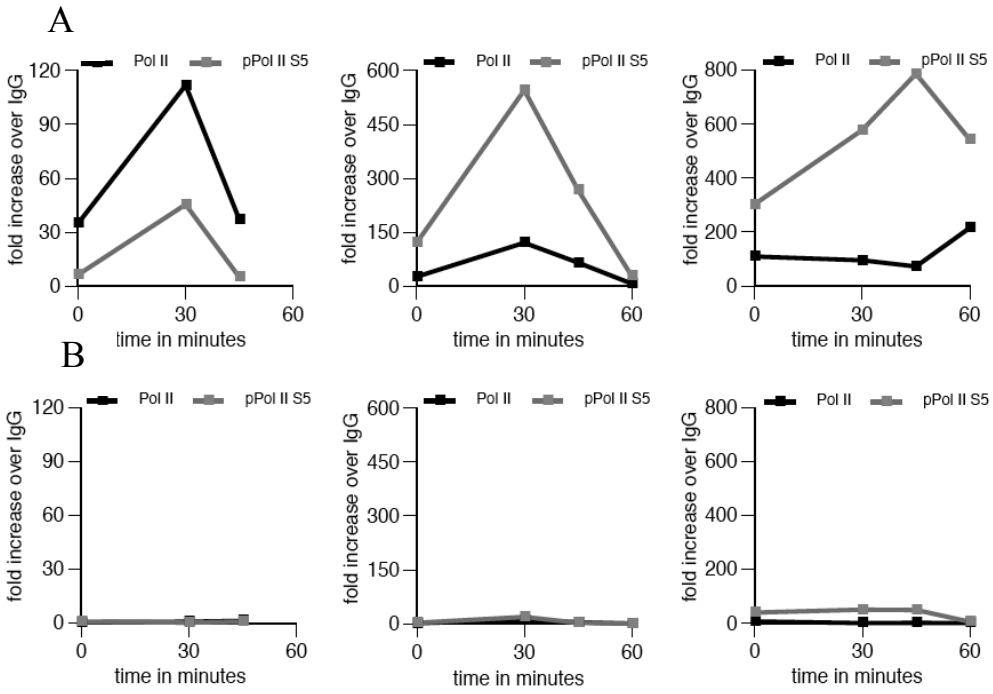

Figure 4.S.12: Polymerase abundance on the transcription start site (TSS). Example of single repeat time courses of ligand-dependent polymerase binding to *ADRP* TSS (A) or a negative control region (B). ChIP assay with antibodies against PolII (A) or pPol II S5 (B) were performed on chromatin extracts from HepG2 cells treated with GW501516 for the indicated times. Analyses were performed by real-time PCR with primers listed in Table 4.S.2. Enrichment is shown as a percentage of input rescued with the indicated antibody relative to that rescued by the IgG antibody.

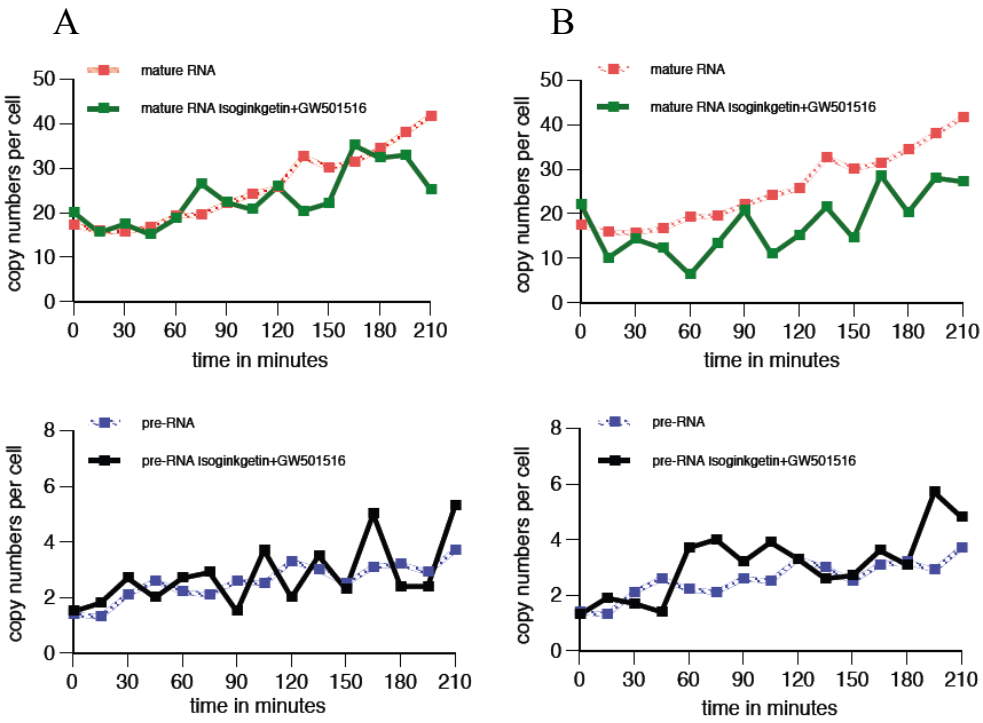

Figure 4.S.13 Splicing inhibition. Human HepG2 cells were incubated with 100 µM isoginkgetin and with PPARδ ligand GW501516 simultaneously (A) or pre-treated for 3h with 100-µM isoginkgetin before adding the ligand for the indicated time (B). The control was mock treatment -medium vehicle (DMSO) instead of inhibitor/ligand. Quantitative real-time PCR was again performed in order to measure pre- and mature mRNA levels after splicing inhibition and the copynumbers were calculated according to described procedure (section 4.S.2). The experiment was carried out in duplicate.

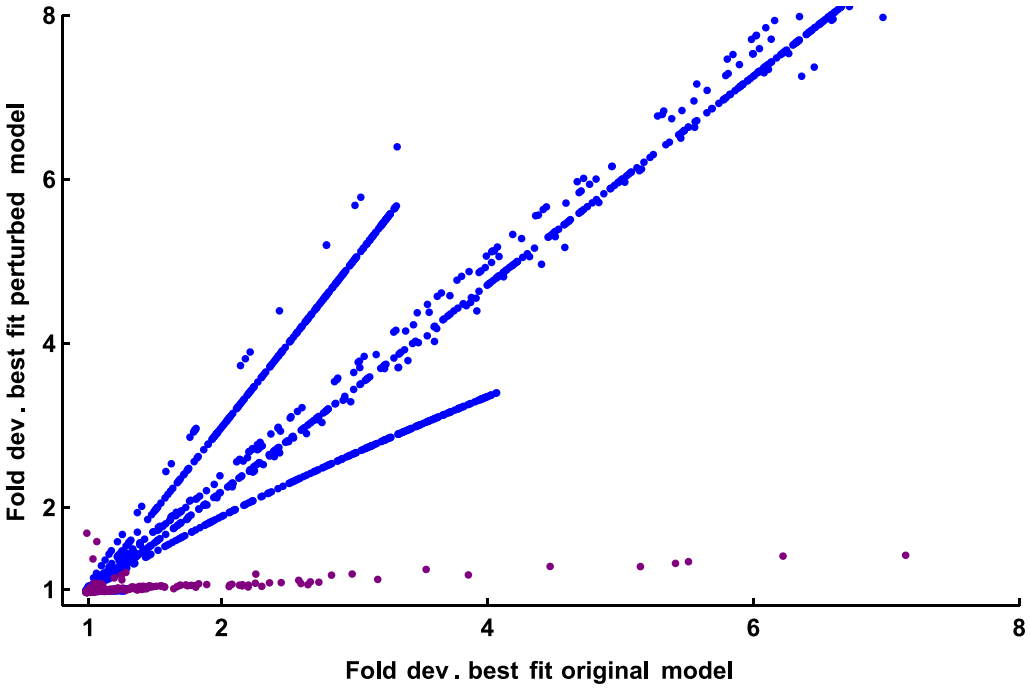

Figure 4.S.14: The effects of parameter perturbation on the splicing inhibition data fitting. Independent parameter changes for all parameters (except k_{spl} and k_{deg})were sampled at random using to the same procedure as for the parameter sensitivity analysis describedin 4.S.5.5.2.. Co-dependent changes in the promoter parameters (k_{act}, k_{ini}, k_{dea} and k_{rev}) were sampled as well according to procedure described in 4.S.5.5.2. The respective fold deviation from the best fits of the original and perturbed models were calculated and plotted against each other. The results obtained with independent parameter sampling are shown in blue; the ones obtained with dependent parameter sampling – in purple.

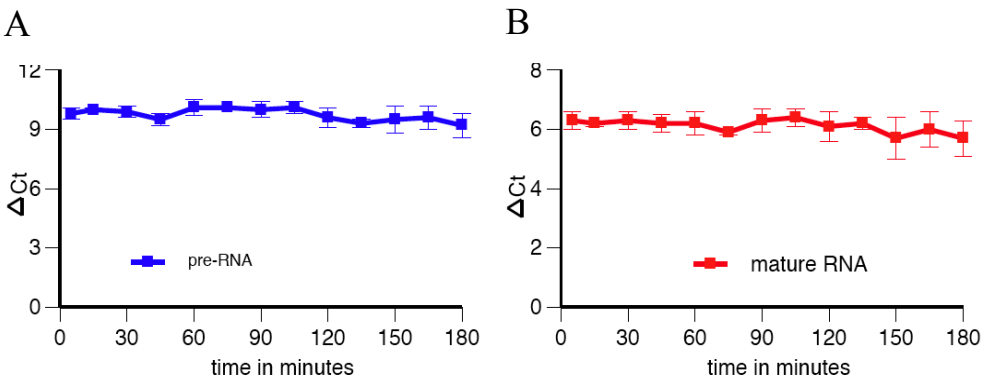

Figure 4.S.15 dM (Ct_{ADRP}-Ct_{RPLP0}) for the DMSO treated samples (pre- and mature RNA) as function of duration of exposure to the DMSO alone. Data points represent averages from three experiments. Bars represent standard deviation.

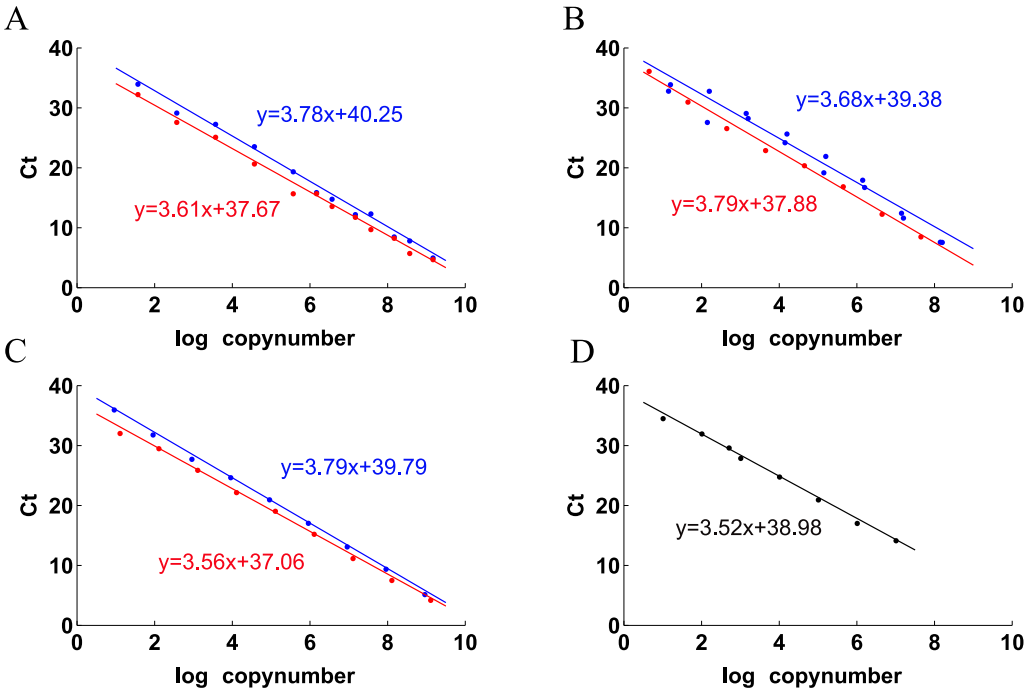

Figure 4.S.16: Standard curves for the absolute mRNA quantification. The qPCR was performed on the known amounts of cDNA fragment; resulting Ct values were plotted against absolute copy number calculated from the measured DNA concentration and individual molecular weights of the standard fragments. In case of ADRP fragments two independent experiments were performed and fitted separately resulting in the maximal (blue) and minimal (red) fits used to estimate the method error. The fit to all data points (not shown) was used to calculate the average copy number. The standard curves were obtained for intron 1-exon1 (A), exon1-exon3 (B), exon5-exon6 (C) and barnase (D) fragments. Log refers to the 10-based logarithm whereas Ct is 2-log based. The theoretical value of the direction coefficient is thereby $-^{2}\log 10=-3.32$.

References

Aldridge, B.B., Burke, J.M., Lauffenburger, D.A., and Sorger, P.K. (2006). Physicochemical modelling of cell signalling pathways. Nature cell biology *8* , 1195-1203.

AMC (2001). Robust statistics , a method of coping with outliers. In AMC technical brief (Royal Society of Chemistry).

Ashyraliyev, M., Fomekong-Nanfack, Y., Kaandorp, J.A., and Blom, J.G. (2009). Systems biology , parameter estimation for biochemical models. FEBS J *276* , 886-902.

Becker, V., Schilling, M., Bachmann, J., Baumann, U., Raue, A., Maiwald, T., Timmer, J., and Klingmuller, U. (2010). Covering a broad dynamic range , information processing at the erythropoietin receptor. Science *328* , 1404-1408.

Bildirici, I., Roh, C.-R., Schaiff, W.T., Lewkowski, B.M., Nelson, D.M., and Sadovsky, Y. (2003). The Lipid Droplet-Associated Protein Adipophilin Is Expressed in Human Trophoblasts and Is Regulated by Peroxisomal Proliferator-Activated Receptor-γ/Retinoid X Receptor. Journal of Clinical Endocrinology & Metabolism *88* , 6056-6062.

Borisov, N., Aksamitiene, E., Kiyatkin, A., Legewie, S., Berkhout, J., Maiwald, T., Kaimachnikov, N.P., Timmer, J., Hoek, J.B., and Kholodenko, B.N. (2009). Systems-level interactions between insulin-EGF networks amplify mitogenic signaling. Molecular systems biology *5* , 256.

Cedersund, G., and Roll, J. (2009). Systems biology , model based evaluation and comparison of potential explanations for given biological data. The FEBS journal *276* , 903-922.

Chang, B.H., Li, L., Paul, A., Taniguchi, S., Nannegari, V., Heird, W.C., and Chan, L. (2006). Protection against fatty liver but normal adipogenesis in mice lacking adipose differentiation-related protein. Molecular and cellular biology *26* , 1063-1076.

Chubb, J.R., Trcek, T., Shenoy, S.M., and Singer, R.H. (2006). Transcriptional pulsing of a developmental gene. Curr Biol *16* , 1018-1025.

Cooper, T.A., Wan, L., and Dreyfuss, G. (2009). RNA and Disease. Cell 136 , 777-793.

Darzacq, X., Shav-Tal, Y., de Turris, V., Brody, Y., Shenoy, S.M., Phair, R.D., and Singer, R.H. (2007). In vivo dynamics of RNA polymerase II transcription. Nat Struct Mol Biol *14* , 796-806.

Draper, N.R., and Smith, H. (1988). Applied Regression Analysis (New York , John Wiley&Sons, Inc).

Fan, B., Ikuyama, S., Gu, J.-Q., Wei, P., Oyama, J.-i., Inoguchi, T., and Nishimura, J. (2009a). Oleic acid-induced ADRP expression requires both AP-1 and PPAR response elements, and is reduced by Pycnogenol through mRNA degradation in NMuLi liver cells. American Journal of Physiology - Endocrinology And Metabolism *297* , E112-E123.

Kang, Z., Pirskanen, A., Janne, O.A., and Palvimo, J.J. (2002). Involvement of proteasome in the dynamic assembly of the androgen receptor transcription complex. The Journal of biological chemistry *277* , 48366-48371.

Karpova, T.S., Kim, M.J., Spriet, C., Nalley, K., Stasevich, T.J., Kherrouche, Z., Heliot, L., and McNally, J.G. (2008). Concurrent Fast and Slow Cycling of a Transcriptional Activator at an Endogenous Promoter. Science *319* , 466-469.

Kreutz, C., and Timmer, J. (2009). Systems biology , experimental design. The FEBS journal *276* , 923-942.

Licatalosi, D.D., and Darnell, R.B. (2010). RNA processing and its regulation , global insights into biological networks. Nature reviews Genetics *11* , 75-87.

Metivier, R., Penot, G., Hubner, M.R., Reid, G., Brand, H., Kos, M., and Gannon, F. (2003). Estrogen receptor-alpha directs ordered, cyclical, and combinatorial recruitment of cofactors on a natural target promoter. Cell *115* , 751-763.

Moreira, J.M.A., and Holmberg, S. (1998). Nucleosome structure of the yeast CHA1 promoter , analysis of activation-dependent chromatin remodeling of an RNA-polymerase-II-transcribed gene in TBP and RNA pol II mutants defective in vivo in response to acidic activators. EMBO J *17* , 6028-6038.

Müller, B., Blackburn, J., Feijoo, C., Zhao, X., and Smythe, C. (2007). DNA-activated protein kinase functions in a newly observed S phase checkpoint that links histone mRNA abundance with DNA replication. The Journal of Cell Biology *179* , 1385-1398.

Murray, E.L., and Schoenberg, D.R. (2008). Chapter 24 Assays for Determining Poly(A) Tail Length and the Polarity of mRNA Decay in Mammalian Cells. In Methods in Enzymology, E.M. Lynne, and K. Megerditch, eds. (Academic Press), pp. 483-504.

Nelson, D.E., Ihekwaba, A.E., Elliott, M., Johnson, J.R., Gibney, C.A., Foreman, B.E., Nelson, G., See, V., Horton, C.A., Spiller, D.G.*, et al.* (2004). Oscillations in NF-kappaB signaling control the dynamics of gene expression. Science *306* , 704-708.

O'Brien, K., Matlin, A.J., Lowell, A.M., and Moore, M.J. (2008). The biflavonoid isoginkgetin is a general inhibitor of Pre-mRNA splicing. The Journal of biological chemistry *283* , 33147-33154.

Poulos, M.G., Batra, R., Charizanis, K., and Swanson, M.S. (2011). Developments in RNA Splicing and Disease. Cold Spring Harbor Perspectives in Biology *3*.

Price, W.L. (1977). A controlled random search procedure for global optimisation. The Computer Journal *20* , 367-370.

Price, W.L. (1983). Global optimization by controlled random search. Journal of Optimization Theory and Applications *40* , 333-348.

Saramaki, A., Diermeier, S., Kellner, R., Laitinen, H., Vaisanen, S., and Carlberg, C. (2009). Cyclical chromatin looping and transcription factor association on the regulatory regions of the p21 (CDKN1A) gene in response to 1alpha,25-dihydroxyvitamin D3. The Journal of biological chemistry *284,* 8073-8082.

Schmierer, B., Tournier, A.L., Bates, P.A., and Hill, C.S. (2008). Mathematical modeling identifies Smad nucleocytoplasmic shuttling as a dynamic signal-interpreting system. Proceedings of the National Academy of Sciences of the United States of America *105* , 6608-6613.

Schwanhausser, B., Busse, D., Li, N., Dittmar, G., Schuchhardt, J., Wolf, J., Chen, W., and Selbach, M. (2011). Global quantification of mammalian gene expression control. Nature *473* , 337-342.

Singh, J., and Padgett, R.A. (2009). Rates of in situ transcription and splicing in large human genes. Nat Struct Mol Biol *16* , 1128-1133.

Suter, D.M., Molina, N., Gatfield, D., Schneider, K., Schibler, U., and Naef, F. (2011). Mammalian Genes Are Transcribed with Widely Different Bursting Kinetics. Science *332* , 472-474.

Targett-Adams, P., McElwee, M.J., Ehrenborg, E., Gustafsson, M.C., Palmer, C.N., and McLauchlan, J. (2005). A PPAR response element regulates transcription of the gene for human adipose differentiation-related protein. Biochimica et biophysica acta *1728* , 95-104.

Tobin, K.A., Harsem, N.K., Dalen, K.T., Staff, A.C., Nebb, H.I., and Duttaroy, A.K. (2006). Regulation of ADRP expression by long-chain polyunsaturated fatty acids in BeWo cells, a human placental choriocarcinoma cell line. Journal of lipid research *47* , 815-823.

Xu, N., Loflin, P., Chen, C.-Y.A., and Shyu, A.-B. (1998). A broader role for AU-rich element-mediated mRNA turnover revealed by a new transcriptional pulse strategy. Nucleic Acids Research *26* , 558-565.

Yankulov, K., Yamashita, K., Roy, R., Egly, J.-M., and Bentley, D.L. (1995). The Transcriptional Elongation Inhibitor 5,6-Dichloro-1-β-D-ribofuranosylbenzimidazole Inhibits Transcription Factor IIH-associated Protein Kinase. Journal of Biological Chemistry *270* , 23922-23925.